EXPERIMENTAL AND ANALYTICAL ANALYSIS OF THE STRESS-STRAIN DIAGRAM OF FRP-CONFINED CONCRETE WITH DIFFERENT LOADING RATES

by

BRANDY SUTHERLAND

B.S., Kansas State University, 2006

A THESIS

submitted in partial fulfillment of the requirements for the degree

MASTER OF SCIENCE

Department of Civil Engineering
College of Engineering

KANSAS STATE UNIVERSITY
Manhattan, Kansas

2007

Approved by:

Major Professor
Asad Esmaeily

Abstract

The accuracy and applicability of the existing stress-strain models for concrete confined by Carbon Fiber Reinforced Polymer (CFRP) were analytically and experimentally explored. This investigation includes major parameters affecting the stress-strain response of confined concrete, including the loading pattern and protocol. It has been observed and reported that the experimentally recorded stress-strain relationship of the same specimen will be different if the loading protocol of the test is switched from displacement control to load control.

In the experimental phase of this study, four standard 6” by 12” concrete cylinders were constructed using the same concrete batch for consistency. Three two-inch strain gauges were affixed equally spaced at mid-height on the surface of the specimen in the longitudinal direction, and two two-inch strain gauges were applied in the lateral direction at mid-height opposite each other. CFRP was then impregnated with a two-part epoxy and applied externally in two continuous layers, with an overlap.

During the first phase of the experimental program, the tests were conducted with a constant load rate or with a constant displacement rate. The data was collected from externally mounted strain gauges and potentiometers positioned on the opposite sides of the cylinder in the longitudinal direction.

Since the capacity of the existing actuator in the structural lab was less than the required failure level of the specimens, a nutcracker-like device was constructed to increase the mechanical advantage of the test frame in the second phase of the experimental program. In this phase, all tests were conducted in displacement control.

Various models were selected to be studied from a large number of existing models that propose to determine the stress-strain relationship of concrete. Analytical predictions of the models were compared against the experimental data. Results show that some of the models provide a reasonable prediction of the real performance of the

specimen. However, in general, predictions are different from the real performance for most models.

Table of Contents

List of Figures

List of Tables

Acknowledgements

Acknowledgement to my advisor, Dr. Asad Esmaeily, is necessary for providing the crucial means to conduct this research and for helping apply for fellowships. After a few problems with my program of study made me wonder if I was ever going to be able to graduate and had me sweating bullets for a short while, he played a key role in reassuring me that I would graduate when I planned.

I am grateful to the faculty members who have agreed to sit on my committee. Dr. Robert Peterman has given honest opinions when approached without appointments and Dr. Sutton Stephens who has given essential advice. Both have been great professors and have always had open doors for questions or just to talk.

Special thanks are also appropriate to Colonel Steve Hart, Dr. Brian Coon, Mrs. Lora Boyer and Mr. Jon Tveite as well as the rest of the McNair staff. The involvement and assistance of Colonel Steve Hart, Ph.D. candidate, throughout the entire process of testing and writing has been insightful and invaluable. The conversations were entertaining and informative and seemed to make the time fly. Thanks to Dr. Coon who has smoothed out the technical problems I encountered. He has voluntarily subjected himself to reading and editing my thesis and has taken a personal interest in my welfare. He has added a great deal of incite about proper English usage and history, keeping the stressful writing process as delightful as possible. The Lora and Jon as well as the rest of the McNair's staff have also been important throughout the editing process.

Thanks are also due to Professor Kimberly Kramer who has become a great friend throughout my time at Kansas State University, whose opinion I value greatly. She was ready to lend a hand and an ear regardless of the problem. I would also like to thank my family, especially my husband Scott, for constantly being supportive and always knowing when I needed a little extra encouragement. Thanks to all who have been there to give the strength and encouragement that I needed to help make this possible.

Preface

As an undergraduate student at Kansas State University, in the Civil Engineering Department, I was accepted into the McNair Scholars Program. One of the requirements for being a member of this program was involvement in a research project in my field of study. I had to submit progress reports periodically in addition to a final report as well as give a presentation over the research material and final project.

At the time, by recommendation of the department head, I started working closely with Colonel Steve Hart, a Ph. D. graduate student, supervised by Dr. Esmaeily. Colonel Hart was working on confined concrete, in general, and more specifically, CFRP-confined concrete. Cyclic stress-strain performance of confined concrete and behavior of CFRP-confined concrete under sustained load was being investigated. I helped with the tests conducted on the CFRP specimens with the purpose of exploring a recently proposed model for cyclic stress-strain relationship of confined concrete prediction (Sakai, 2006).

After I graduated with my Bachelor of Science degree from the Civil Engineering Department, I continued to get my Master of Science degree and followed my research activities on the same path as I had started in terms of confined concrete and its related issues. I continued my work with the same research group as I had started earlier, but selected to explore the validity, accuracy and applicability of the representative models proposed by different researchers for monotonic stress-strain relationship of concrete confined by CFRP. Following is a report on analytically and experimental parts of my work and the pertinent conclusion.

CHAPTER 1 - Introduction

Concrete is one of the most popular and commonly used construction materials all over the world. The main ingredients of concrete are widely available. The technology to prepare concrete is relatively simple compared to other construction materials. Concrete is known to have been used since the time of the Greeks and Romans (Nawy, 2005), but the comprehensive study of concrete started in the late 18^{th} century and early 19^{th} centuries. In 1756, John Smeaton used pozzolana mixed with clayey limestone; this gave way to the first understanding of the chemical properties of hydraulic lime (Neville, 1997). In 1801, a paper was published acknowledging the disadvantages of trying to use concrete in tension (Nawy, 2005).

Concrete is made up of cement (usually Portland cement, but Fly Ash and Slag Cement can also be used), and typically sand or manufactured sand and gravel limestone or granite make up the fine and coarse aggregates, respectively, with water and admixtures completing the conglomeration. The chemical process known as hydration causes the materials mentioned above to chemically bond to each other and harden, creating the heterogeneous material known as concrete, but often referred to as cement by the general public (Taylor, 1997).

The use of concrete for construction of structural elements has both advantages and disadvantages. The advantages are the relatively inexpensiveness of the materials, a variety of uses and application processes, the ease of placement allows for a number of different shapes and designs, and the high compressive strength is great for structural integrity. The time required allowing the concrete to properly cure for the necessary strength, the time required to place the forms, the lack of tensile strength, in addition to the lack of constant behavior due to the variations in the material constituents are primary disadvantages of concrete.

Plain concrete has a good compressive strength, but a poor tensile strength and low ductility. Plain concrete has a high tolerance for compressive forces; however, it performs poorly when a force is applied in tension. The tensile strength of commonly used concrete is between one-tenth and one-fifth and is specified by ACI as $7.5\sqrt{f'_c}$

(Nawy, 2005) of the concrete's compressive strength, hence, is generally ignored in the design process. To address this deficiency, concrete is reinforced with a material that has a high tensile strength, such as steel. The idea of reinforced concrete has been around since 1850 when Jean-Louis Lambot constructed a rowboat; this was the first application of reinforced concrete (Loov, 1991). However, a Parisian gardener, F. Joseph Monier, patented the metal frames used as reinforcement for flowerpots in 1865, after placing cement around a wire frame of a planter to help with stability (Nawy, 2005). To combat the low tensile strength, steel is added to the concrete in the sections of the member where tension will occur. These steel bars are called rebar and are used for shear and tensile reinforcement in the parts where tension is expected to take place. The spacing and size of the reinforcing bars is determined based on the amount of tension in the member. Once the longitudinal reinforcement is in place, the plain concrete becomes reinforced concrete. However, there are some other concerns with concrete, even when reinforced with a material that has a high tensile strength.

A reinforced concrete structural member, such as a beam, even when reinforced in longitudinal direction, is brittle compared to steel. Because of this brittleness, the ductility of the member, and in turn, of the reinforced concrete structure, is limited. Ductility is one of the basic requirements for a structure to withstand dynamic loading, such as those experienced during an earthquake. Reinforcement is also used to control some of the cracking that can occur as a result of temperature changes. A thermal coefficient of expansion is used to control this cracking.

To improve the behavior of reinforced concrete in terms of ductility, confinement can be provided by steel in the transverse direction, or with other materials such as Fiber Reinforced Polymer (FRP). FRPs are usually applied on the surface of the member by some kind of adhesive material. Confined concrete has more compressive strength and ductility when compared with plain concrete.

In the early experiments and models, application of the lateral pressure was achieved by using hydrostatic pressure. In 1906, the effect of lateral pressure in enhancement of compressive strength and deformation capacity of reinforced concrete, or ductility was documented by some researchers (De Lorenzis, 2001). Confinement is defined as restricting the lateral dilation of concrete. This initially was accomplished by

using “transverse reinforcement in the form of spirals, circular hoops or rectangular ties, or by encasing the concrete columns into steel tubes that act as permanent formwork” (De Lorenzis, 2001). Confinement allows for enhancement in concrete strength and deformation. The innovation of FRP allowed for materials other than steel to be used as confinement. FRP is available in many forms from different materials. The FRP allows the concrete to be externally wrapped with sheets, tapes or tubes. The most common materials used for FRP are carbon, glass and Aramid. Glass Fiber Reinforced Polymer (GFRP), Carbon Fiber Reinforced Polymer (CFRP) and many other types of reinforcing fibers have been used to retrofit the existing reinforced concrete structural members to enhance their force and displacement capacities, or in new structures to increase their strength, ductility and their resistance against environment.

Understanding the behavior of any construction material is the stepping stone in design guidelines. The monotonic and cyclic stress-strain response of plain concrete as well as concrete confined by conventional reinforcement or FRP plays a key role in the response of structural members and in turn the whole structure when exposed to various loading conditions. It is important to better understand the properties and behavior of concrete, so that design of concrete structures and structural elements is possible. The understanding of the behavior of concrete is greatly desired, thus the continued study allows those engrossed in the behavior to construct models that may be used in the future to accurately predict the behavior of concrete. The goal of accurately predicting the stress-strain response of confined concrete keeps researchers striving to improve the existing models or to make new models that have more correctly predicted results.

These many models, studies, and theories reveal that many factors have an effect on the stress-strain diagram of concrete. Some of these items have been identified in the various existing models, but due to the number of items influencing the diagrams, only selected parameters are chosen to be evaluated depending on the scope of the model. These parameters can include the following: testing conditions (type of machine, loading rate, duration of load, and load history), physical parameters of the specimens (such as size and shape), the size and location of strain gauges, the number of cycles, the age of the concrete, and the material makeup of the concrete including type and quantity of aggregate, as well as concrete strength (Popovics, 1973).

Many models exist to evaluate reinforced and confined concrete. Some of the different parameters incorporated in confinement models include the type of confinement, such as traditional steel type—spirals and hoops, rectilinear ties and concrete filled-steel tubular columns—and FRP. Mander et al (1988) was the first to establish a way to derive a process to model the stress-strain relationship for circular and rectangular reinforced concrete sections confined by conventional reinforcement (Lorenzis, 2001). Loading pattern and loading history, cyclic and monotonic loading patterns, reinforcement type and material, material properties of the concrete and the reinforcement, concrete and steel strength and ductility of each are all variables considered in existing models.

In this study, the experimental test data will be compared with several models to determine the validity of the models. The comparison with Mansur et al (1994) will be made to determine if the correction factors proposed are appropriate. The correction factor is designed to adjust for the effect of the deformation of the entire system, as opposed to the deformation of only the specimen. The intent is to determine whether the correction factor will be valid when FRP-confined concrete is used as the specimen. This is necessary because the model design was based on unconfined, plain concrete. This idea will be compared with the experimental data.

According to the model proposed by Popovics (1973), the initial modulus of elasticity for concrete tested at a constant stress rate will result in a higher slope than that of concrete tested at a constant strain rate. This theory will be compared with the experimental test data. Also, the equations submitted for determining the shape of the stress-strain curve will be used to evaluate the model's ability to predict the stress-strain diagram for confined concrete. Since not all of the equations have been justified by experimental data, the goal will be to prove or disprove that legitimacy of the equations provided in the model as proposed by Popovics. This model, too, was created based on plain, unconfined concrete.

Toutanji (1999) proposed a model to predict the stress-strain curves of concrete externally confined with FRP sheets. The specimens used to create the model were loaded with a constant stress. This model calculates the second branch of the stress-strain diagram first. Then the equations for the first branch are provided based on an equation

proposed by Ahmad and Shah. Finally, the transition point is determined which indicates when the equations for stress and strain and the values for first branch become invalid, and when the equations for stress and strain and the values for the second branch become valid. The experimental data is then compared with the predicted stress and strain values from the model.

The model proposed by Berthet et al (2006) first predicts the ultimate stress and ultimate strain of concreted confined by externally applied composite jackets. This proposed model is based on an equation proposed by Toutanji (1999) which is used to calculate the stress in the first branch. The expected ultimate stress is used to calculate the transition point between the first and second branch. Then, an axial strain corresponding to the radial strain of 0.002 inch/inch is calculated. Once the transition strain and stress are calculated, the second branch can be determined from the stress and strain equal to and greater than that of the transition stress and strain values. The stress for the first branch is then calculated and displayed with the corresponding strain up to the transition stress and strain.

Teng and Lam (2003, 2004) compare the results from design-oriented models and analysis-oriented models. They then propose a design-oriented model compiled by test data from open literature based on the four parameters by Richard and Abbot. The use of analysis-oriented models to help with the correlation between the FRP jacket stiffness and that of the concrete assisted in the prediction of the ultimate confined strain. This model uses simple equations breaking up the first and second branch, with two equations at a transition strain based on the modulus of elasticity of second branch based on the ultimate confined stress, the reference stress and the ultimate strain. The ultimate strain is calculated using the manufacturer's values for ultimate tensile strength, even though the data does not support that idea, because an FRP efficiency ratio was determined based on the data from the open literature. This FRP efficiency fact was then applied to the ultimate confined stress.

Each of the above-mentioned models will be discussed in great detail in the following chapters. The experimental program for the experimental data which will be used to compare with the above models will be specified. The experimental data will be

compared with the predicted values of the stress-strain diagrams. Finally, the results of the comparison will be discussed, as well as the validity of the proposed models.

Objective

The intent of the research is to evaluate—both experimentally and analytically—the stress-strain relationship of FRP-confined concrete under monotonic loading. This evaluation included the experimental response of confined concrete under a monotonic load and investigation of the accuracy and applicability of some representative analytical models proposed by various researchers for confined concrete. The loading type was either at a constant rate of stress or at a constant rate of strain, commonly referred as force-controlled or displacement-controlled loading, respectively. The constant load rate or constant displacement rate was determined based on the ASTM standards for testing concrete, as well as from information provided in existing models and experience from tests previously conducted.

The performance of the samples tested under a pre-defined loading scenario and the complete stress-strain diagrams showing this performance are presented. The diagrams compare the experimental test results as well as the stresses and strains predicted by the existing models having similar test parameters. This comparison will determine whether the equations and modifications applied to some of the existing models are reasonable adequate, or if additional modifications are necessary to enhance the models' predictions.

Background

The idea of confined concrete has been around since 1906, when Considère saw that there was added benefit in strength and deformation when hydrostatic pressure was applied to concrete (Lorenzis, 2001). Richart et al determined that the confined axial strength compared to that of unconfined was about 4.1 times the confining pressure value (Lorenzis, 2001). Richart et al also performed the test with continuous steel spirals providing the confining pressure and compared the results with the results from the previous test: the results were confirmed; others have found this ratio to be as low as 2.8 and as high as 7.0 (Lorenzis, 2001).

Confinement type has changed over the years. Traditionally, steel hoops, ties, or spirals have been used; however, with the innovation of FRP, the use of this material has increased. The increase is in part due to the inherent properties of FRP, such as extremely high strength-to-weight ratio, high tensile strength and modulus, good corrosion behavior, electromagnetic neutrality, durability, and its ease of use for multiple applications in new construction; FRP is also used for retrofitting on multiple types of structural materials like wood or masonry (Lorenzis, 2001). FRP can be used to preserve many structures that have sustained damage over time due to environmental conditions, such as damage encountered due to seismic activity, or change in the function of the structure from its original intended use from being rebuilt. However, because there are many models that exist, and most do not give a numeric evaluation of the performance of FRP-confined concrete, the behavior of FRP-confined concrete is important to be studied further so that a valuable, accurate model can be determined—one that will result in a better design aid when concrete structures are planned and designed.

Popovics (1973) discussed the stress-strain diagram when the load is applied at a constant stress as opposed to a constant strain. Formulas that can be found in the literature take into consideration the strength of concrete when comparing the initial modulus of elasticity to the secant modulus of elasticity at the ultimate stress. However, these formulas are only valid for standard specimens with a height-to-width ratio equal to or greater than two and when the load is a short-term load applied at a rate that produces a constant rate of strain in the specimen (loaded in displacement or deformation control). Experimental data has yet to support these formulas.

It has been seen in unconfined concrete that the curvature of the stress-strain diagram increases with the amount of aggregate in the concrete because there is friction at the interface of the aggregates within the concrete mix; however, the water-to-cement ratio, curing and age do not play a significant role—if any—in the relative deformation (percentage) in the stress-strain diagram. However, it may contribute a great deal to the overall strength (Popovics, 1970).

A complete compressive stress-strain relationship is modeled by Mansur et al (1994) in a closed-loop, servo-controlled hydraulic testing machine using plain, unconfined concrete. This model determines a correction factor so that the strain, as

measured globally (over the total length of the specimen), can be correlated to the strain at the central region of the specimen, where the actual strains are evident per Saint Venant's principle. This is needed because there are intrinsic errors in the strain when measured globally due to frictional resistance at the end restraints, as well as the interaction between the specimen and the testing machine.

For plain, unconfined concrete, once the peak strain is reached and microcracking begins, it may not be possible to determine the local strain from the central region of the specimens and the deformation may have to be measured from transducers located at the end plates. The data from the transducers after peak strain has been reached includes the deformation of the specimen as well as the mechanical compliance (Mansur et al, 1994). To take into consideration the machine deformation, a correction factor was proposed.

A design-oriented model intended to predict the entire stress-strain relationship of concrete confined with FRP sheets was presented by Tountanji (1999). This model is a function of the confining stress based on the radial strain, the modulus of the FRP and the geometric function of the concrete and FRP. Then, the corresponding axial stress for the second branch of the stress-strain curve was calculated, followed by the axial strain. Finally, an equation for the stress for the first branch is given, followed by the stress and strain at the transition point for the intersection of the first and second branches.

An analytical model introduced by Berthet et al (2006) considers the confinement level, as well as the FRP mechanical properties, to evaluate the ultimate capacity and the stress-strain relationship as a function of the concrete and confining material. This model first predicts the ultimate values for stress and strain, then determines the formulation for the linear second branch, as well as the transition point between the first and second branches. Finally, the first branch is determined.

The ultimate stress is determined as a function of the lateral confining stress. The ultimate strain can be ascertained as a function based on a ratio of the confinement modulus and the ultimate unconfined stress, the manufacturer's value for ultimate FRP strain, Poisson's ratio, and the axial strain. The slope of the second branch is established based on a regression line, which is used to determine the stress at the transition point as well as the stress for every point greater than that of the transition strain. The first branch is shaped by an equation used by Toutanji (1999) based on an equivalent modulus of

elasticity corresponding to the axial strain to calculate the stress and axial strain pairing with the assumed maximum radial strain of 0.002 inch/inch.

CHAPTER 2 - Discussion of the Existing Models

Overview

So far, the early models discussed have been for unconfined concrete. Although the ascending branch is nearly identical for confined and unconfined concrete, once the peak unconfined stress and strain are reached, the behavior varies, depending on which model one follows. Some models even begin to deviate from the ascending branch of the unconfined concrete once the linear portion of the stress-strain diagram are passed, due to the principle that the FRP is beginning to become engaged once there is cracking within the core concrete.

A stress-strain diagram proposed by Popovics (1973) is intended to address the concern that loading at a constant stress, as opposed to loading at a constant strain, will result in a stress-strain curve that has a stiffer initial modulus of elasticity for specimens loaded at a constant stress. This model and the correction factors and equations were established based on plain, unconfined concrete. Some of the equations have not been verified with experimental data and are only applicable to specimens that have a height-to-width ratio of two or more.

Mansur et al (1994) tested plain, unconfined concrete specimens in displacement control at a rate of 0.00276 inches/minute, with strains being collected over the entire length of the specimens as well as at the central portion. The strain must be collected from the central portion of the specimens because once the peak values are reached for unconfined concrete, the strain can no longer be collected from the central portion due to concrete failure. Thus, the deformation must be collected globally, which included the deformation of the concrete, in addition to the end resistance and machine deformation being measured from the transducers. Correcting the additional deformation to what would be measured at the central portion allows for the strain to be estimated even though it is not directly measured.

Toutanji (1999) provides an analytical model to predict the stress-strain diagram for FRP-confined concrete based on "deformation compatibility and equilibrium for forces between concrete and FRP composites" (p 397). Loading was applied at a rate of 32 psi/sec, while the experimental testing was conducted at 35 psi/sec per ASTM C-469. Although the loading rate appears to nearly identical, the specimens are three inches in diameter as opposed to six inches. Thus, the load rate is about 13.5 kips/minute, while the test data was loaded at a rate of 60 kips/minute. This results in a difference of a factor of four in the load rate of the experimental test data and the way the data was collected for the model. This is the first of the confined models with which test data will be compared.

Berthet et al (2004, 2005) conducted tests on FRP-confined concrete at a loading rate that was about equal to that of the loading rate of the experimental tests. The tests conducted by Berthet et al had a loading rate of 0.00787 inches/minute, which was close when compared to the experimental testing which had a loading rate of 0.0068 inches/minute during the first round of tests. Transducers and gauges were applied at mid-height on the specimens to measure the strain.

Teng and Lam (2004) have compared several existing FRP—design-oriented and analysis-oriented—models as well as proposed a new model. The Lam and Teng model (2003), although very thorough in comparisons, did not report a load rate; however, it was ascertained by contacting the authors that the loading rate was about 0.0236 inches/minute. It should be mentioned that it would have been ideal to also compare different loading patterns when loading in force control. However, not many models were constructed based on experimental results in force control mode, and in the few available models, the loading rate was nearly identical to that of the test data.

Popovics (1973)

To take into consideration that the strength of the concrete plays a key role in the shape of the stress-strain diagram, Equation 1 allows for the ratio of the initial modulus of elasticity to the secant modulus of elasticity at the ultimate stress (E/E_o) to vary depending on the compressive strength of the concrete. The equation is then used to calculate the stress for a given strain value,

Equation 1

$$f = E\varepsilon\left(\frac{n-1}{n-1+\left(\frac{\varepsilon}{\varepsilon_o}\right)^n}\right)$$

where f = axial stress, E = initial modulus of elasticity, ε = strain, ε_o = strain at ultimate stress (f_o), n = function of compressive strength of normal weight concrete given by Equation 2 as follows:

Equation 2

$$n_{concrete} = 0.4x10^{-3} f_o + 1.0$$

Equations similar to Equation 2 are available for mortars and pastes, but were not used in this paper or in the analysis of the experimental data, and thus were not reported but can be found in the literature. When $\varepsilon = \varepsilon_o$ the relationship for the modulus of elasticity becomes Equation 3.

Equation 3

$$E = \left(\frac{f_o}{\varepsilon_o}\right)\left(\frac{n}{n-1}\right)$$

Now, Equation 4 is a variation of Equation 1 with the adjusted modulus based on the ultimate strain,

Equation 4

$$f = \varepsilon\left(\frac{f_o}{\varepsilon_o}\right)\left(\frac{n}{n-1+\left(\frac{\varepsilon}{\varepsilon_o}\right)^n}\right)$$

where f_o = ultimate stress and all other variable remain the same as Equation 1. Here it should be noted that the author indicates the above-mentioned formulas are only valid for standard concrete specimens with a height-to-width ratio of at least two, and when the "uniaxial compressive load is a short-term load which is applied at a rate that produces constant rate of strain in the specimen" (Popovics 1973, p 588). Figure 2.1 shows the expected stress-strain diagram for the situation where the rate of displacement is kept

constant, resulting in the bottom curve while the top curve is for specimens that have a constant load rate applied.

Figure 2.1: Stress-strain curves comparing constant stress with constant strain

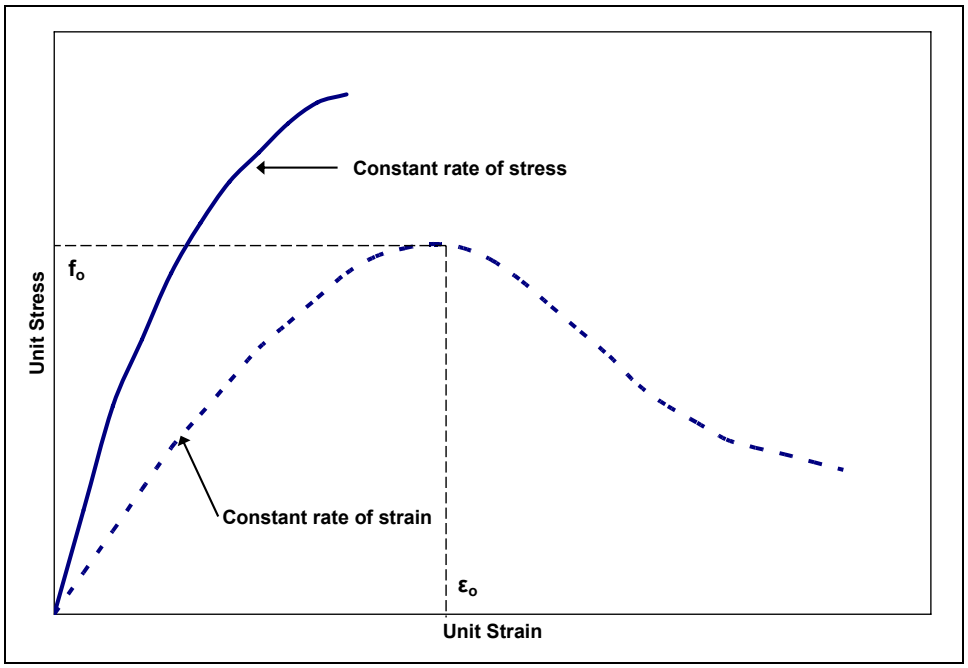

The reliability of the equations above has not yet been confirmed by experimental data. Therefore, the equations will be compared with experimental data based on two situations. The first is that both f_o and ε_o are known from the experimental data. However, it is rare that experimental data is available during the design process; it is more likely that the only information available is f_o, thus, the second situation.

For situations in which both f_o and ε_o are known, these values should be used in Equation 4 to predict the stress from the strain. Table 2.1 shows the sample label name for each of the specimens. This table explains the meanings for the sample label names, in addition to giving valuable information regarding the testing method for each specimen during the two rounds of testing, as well as the loading rate of the specimens. With the information provided in the table below, the charts displaying the test data and the data from the model predictions will be better understood, as can be seen in Figure 2.2 and the remaining figures. Figure 2.2 shows the test data of four specimens compared with the stress predicted by Equation 4 with the appropriate associating strain. The ultimate stress and corresponding ultimate strain were known from the experimental testing. Since this model is for unconfined concrete the maximum stress is that of unconfined concrete.

Table 2.1: Specimen labels, label meanings, testing method and loading rate

Sample Name	Meaning	Testing Method	Loading Rate
B1 fc	#1: 1st Round	Force Control	60 k/min
B2 fc	#2: 1st Round	Force Control	60 k/min
B3 dc	#3: 1st Round	Displacement Control	0.0068 in/min
B4 dc	#4: 1st Round	Displacement Control	0.0068 in/min
B1s	#1: 2nd Round	Displacement Control	0.0167 in/min
B2s	#2: 2nd Round	Displacement Control	0.0167 in/min
B3s	#3: 2nd Round	Displacement Control	0.0167 in/min
B4s	#4: 2nd Round	Displacement Control	0.0167 in/min

Figure 2.2: Comparison of test data with f_o & ε_o used for construction of the curves

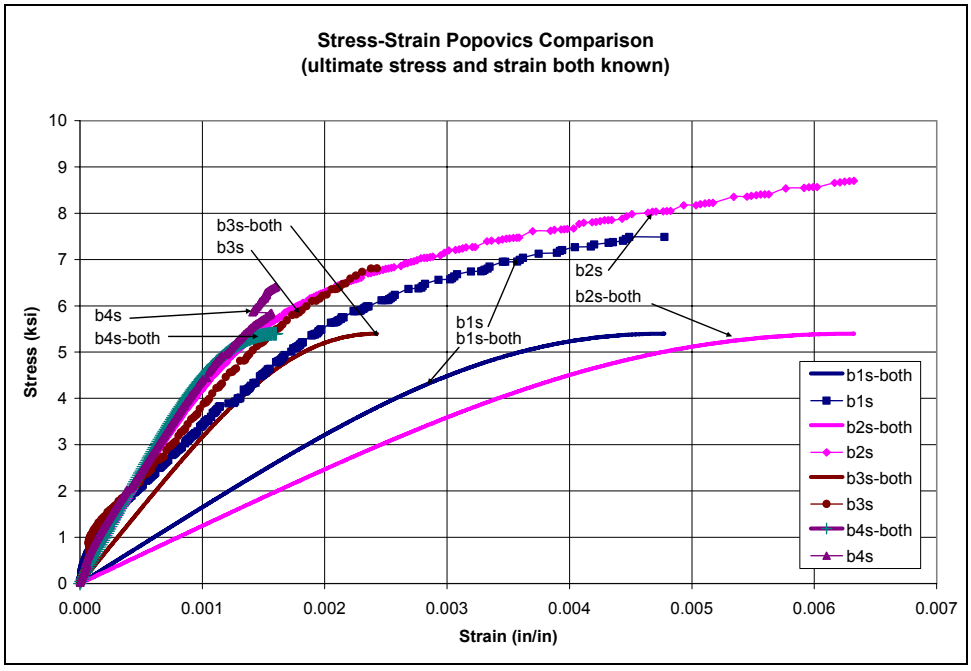

For illustrating the stress-strain diagram when only the ultimate stress is known Equation 5 is used to determine what the ultimate strain will be based on the ultimate unconfined compressive strength,

Equation 5

$$\varepsilon_o = \frac{k\sqrt[4]{f_o}}{10000}$$

"where *k* is a function of the type of mineral aggregate used and the applied test method" (Popovics, 1973, p 592). Since the coefficient *k* is a function of the concrete material and testing method, Table 2.2 was compiled based on the experimental data relationship of strain to stress. The coefficient of determination ranges from about 81% to 99.5% with the mode *k* value being 3 $in^{1/2}/lb^{1/4}$ and a mean value of 3 $in^{1/2}/lb^{1/4}$ for the first round of experimental tests and 4 $in^{1/2}/lb^{1/4}$ for the second round.

Table 2.2: Experimental *k* values

Sample	k value ($in^{1/2}/lb^{1/4}$)	R^2 (%)
B1 fc	3	99.34
B2 fc	3	99.46
B3 dc	3	99.30
B4 dc	3	99.12
Average	3	98.68
B1s	5	92.34
B2s	6	81.22
B3s	3	97.13
B4s	3	99.30
Average	4	80.99

Equation 5 was used with the appropriate *k* values determined from the experimental data, in conjunction with Equation 4, to determine the stress-strain diagram for one of the four specimens. The first and second rounds of test data for one specimen were used to construct Figure 2.3, which shows the comparison between the stress-strain curves if both the ultimate stress and ultimate strain are known (shown as solid lines), and when only the ultimate stress is known (shown as dotted lines) with that of the experimental data (represented by data points smoothly connected). The experimental data from the first round of tests was collected at a constant stress, while the second round of tests was collected at a constant strain.

Similarly, Figure 2.4 shows the relationship of the predicted stress-strain curves based on the ultimate stress and strain being known, compared with the predicted stress-strain curves based solely on the ultimate stress. These predictions were then compared with the experimental data from one of the three remaining specimens. The difference between the two figures, besides the fact that different specimens were used, is that

during both rounds of tests, the loading was such that a constant rate of strain was applied throughout that particular test. So, the strain rate for each round was constant, even if the rate for each round was different from one specimen to the other.

Figure 2.3: Test & theoretical data where f_o & ε_o are known and only f_o is known

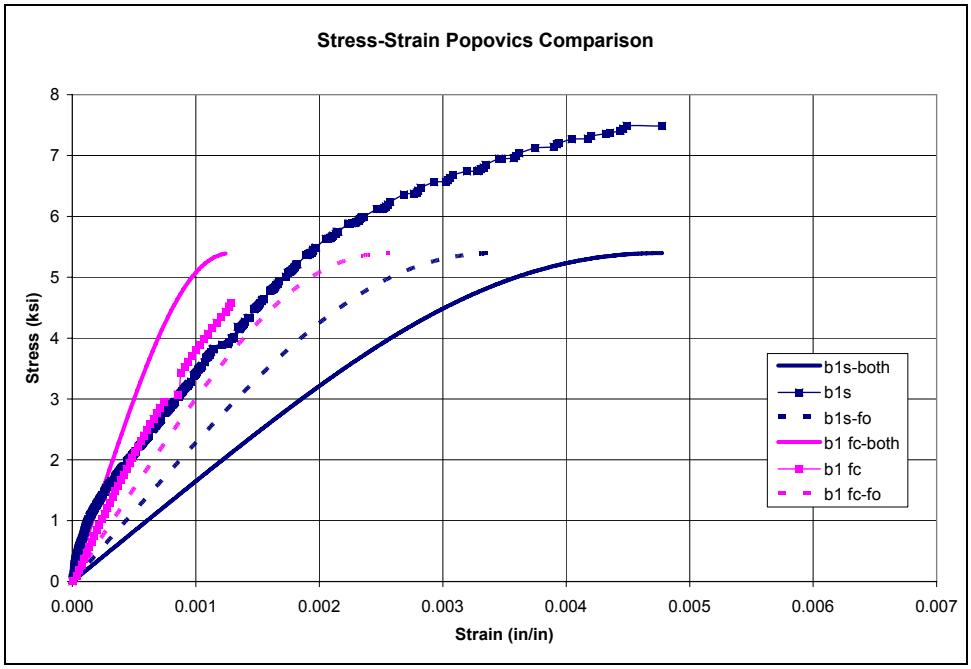

Figure 2.4: Test data & predicted curves for both rounds of tests when f_o & ε_o are both known as well as when only the f_o is known

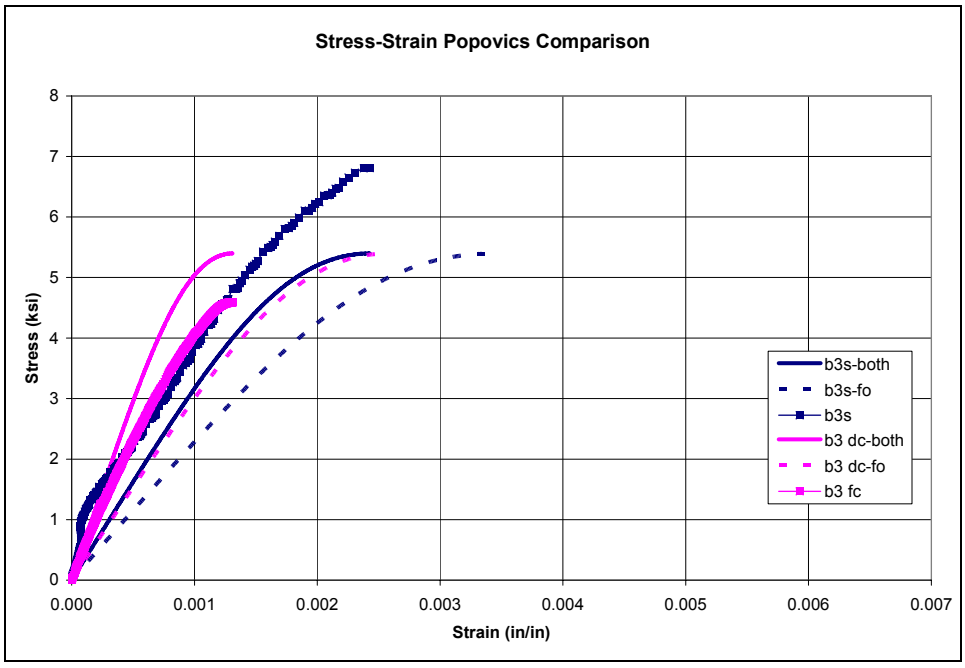

The complete results from the modeling will be discussed in greater detail in another section of this paper. There will also be discussion about any conclusions that can be drawn about this model as well as any recommendations for improving the model, if any, are possible or needed.

Mansur et al (1994)

Because there is deformation in the testing system as well as in the concrete specimens, a correction factor to take this into consideration was established by Mansur et al (1994). This correction factor will allow for deformation to be measured from the platens of the testing machine and will adjust for any machine compliance as well as end-zone effects. To determine the correction factor a "large number" of unconfined plain concrete cylinder and prism specimens with varying compressive strengths were tested (Mansur et al, 1994, p 286). The specimens varied from 4-inch-by-8-inch cylinders to 4 inch by 4-inch-by-8-inch prisms with loads ranging from about 7.25 ksi to 18.85 ksi. The tests were conducted in a closed-loop-servo-controlled hydraulic testing machine that had a maximum capacity of about 675 kip $_{(force)}$. A pair of displacement transducers controlled the displacement rates, which range from 0.0003937 inches/minute to 0.03937 inches/minute.

The ends of the specimens were milled to ensure a level surface. Four compressometer displacement transducers were directly attached diagonally opposite of each other over the central half of the specimens. Two electrical resistance strain gauges, about 2.3 inches in length, were also applied diagonally over the central portion of the specimens to check the reliability of the transducers. A data logger connected to a computer was used to collect all the strain measurements in addition to displacement and load values from the different equipment.

True axial loading was ensured by preloading each specimen to one-third of its cube strength and adjusting the placement based on the readings from the transducers. The loading rate for specimens that had a compressive strength of less than 13 ksi was approximately 0.002756 inches/minute and about 0.001968 inches/minute for higher compressive strengths. All specimens were loaded until they reached crushing failure.

To know for certain if end-zone effects were unintentionally skewing the transducer readings, two electrical resistance strain gauges were applied at mid-height and compared with the readings from the transducer. It was determined that there were no end-zone effects distorting the strain readings. Because the compressometer transducers are only effective up to the peak load, (because of cracking and spalding of the unconfined concrete), the displacement transducers applied to the platens are critical in gathering the post-peak values. It is here, where the stress-strain relationship based on the central portion of the specimens, differs from the stress-strain relationship based on the displacement transducers mounted on the platens.

Assuming that the testing apparatus will not allow sudden failure and that the local strain values are known up to the peak, the displacement transducer values can be corrected to exhibit an accurate stress-strain relationship. The displacement transducers account for displacement of the central portion of the specimen and the end-zone effects as well as the deformation of the testing machine as is illustrated in Equation 6,

Equation 6

$$\Delta_{dt} = \Delta_c + \Delta_{sys}$$

where Δ_{dt} = deformation measured by the displacement transducer at the machine platens, Δ_c = actual axial deformation of the concrete, and Δ_{sys} = deformation of machine and end-zone effects. Assuming that Δ_{sys} can be calculated based on Equation 7 as a function of applied load, Δ_c can be determined,

Equation 7

$$\Delta_{sys} = \Delta_{dt} - \frac{\Delta_{co}}{L_g} L = \left(\frac{\sigma}{E_{dt}} - \frac{\sigma}{E_{co}} \right) L$$

where Δ_{co} = deformation measured by compressometer over gauge length, L_g, L = distance between machine platens, σ = applied stress, and E_{dt} and E_{co} are the initial tangent moduli of concrete based on the stress-strain diagrams derived from the displacement transducer and compressometer transducer values, respectively.

Rearranging Equation 6 and with Equation 7 substituted for Δ_{sys} the actual axial strain can be calculated and is shown in Equation 8. As a result of dividing Equation 8 by L, the actual axial strain can be determined by using Equation 9,

Equation 8

$$\Delta_c = \Delta_{dt} - \left(\frac{\sigma}{E_{dt}} - \frac{\sigma}{E_{co}} \right) L$$

Equation 9

$$\varepsilon_c = \varepsilon_{dt} - \left(\frac{1}{E_{dt}} - \frac{1}{E_{co}} \right) \sigma$$

where ε_c = actual strain at any stress σ, ε_{dt} = strain measured by the transducers between the machine platens. It should be noted that for the correction to be determined, strain at the central region of the concrete specimens must be available.

Toutanji (1999)

Due to the heavily growing use of FRP with concrete elements and structures, a better understanding of the behavior and performance was needed. In 1999, Toutanji presented the results of experimental and analytical analyses on the performance of concrete columns externally wrapped with FRP. Concrete columns were wrapped with two different types of carbon FRP and one type of glass FRP. They were then loaded in axial compression along with control specimens. There were a total of 18 cylindrical specimens measuring 3 inches by 12 inches, of which 12 were wrapped with FRP, leaving six as the control specimens. The concrete mix had a ratio of cement:sand:gravel:water of 1:2:3:0.5 respectively. There were no additives and Type II Portland cement was used with a crushed stone that had a maximum size of one-half inch. The sand consisted of 50% beach sand and 50% river sand. All specimens were cured for 85 days at a temperature of about 78°F and a relative humidity of more than 90%. The average 28-day compressive strength was about 4.35 ksi.

Two continuous layers of unidirectional FRP impregnated by epoxy-resin were applied to the cylinders. The resin to hardener ratio for the two-part epoxy-resin was 2:1 and was mixed for at least five minutes. The cylinders were washed and dried prior to the application of about 0.75 oz/ft^2 of epoxy was applied to the specimens ensuring good contact throughout the application process. There was about a three inch overlap in the FRP wraps. The specimens were left at room temperature for at least seven days to ensure that the epoxy fully cured.

All specimens were loaded with a uniaxial compressive load with a hydraulic testing system at a constant load rate of about 13.5 kips/minute. The ends of the cylinders were capped with sulfur to ensure a level surface and help evenly distribute the loads applied to the specimens. A load cell was used to determine the load being applied to the specimens. Electronic strain gauges were applied to measure the longitudinal and radial strains at the central portion of the specimens. A computer data-logger was used to collect the load and strain values throughout the tests.

With the assumption that the deformation in the concrete and the FRP confinement are compatible and will produce the same strains, Figure 2.5 is the free-body diagram demonstrating how the lateral stress will be calculated. With this model, the values used in the equations must be in metric units. Based on the equilibrium equations and the deformation compatibility assumption, the lateral stress can be calculated using Equation 10

Equation 10

$$f_l = E_l \varepsilon_l$$

where E_l = lateral elastic modulus and ε_l = lateral strain of the confined specimens. Where E_l is calculated using Equation 11, which represents the stiffness of the confinement,

Equation 11

$$E_l = \frac{E_{frp} t}{R}$$

where E_{frp} = elastic modulus of the FRP as provided by the manufacturer, t = thickness of the FRP, and R = radius of the cylinder. Since the elastic modulus of the epoxy is small in comparison to that of the FRP, it is not considered necessary in calculating the lateral elastic modulus (E_l) of the confined specimens.

Figure 2.5: Cross section of confinement and mechanics produced by FRP

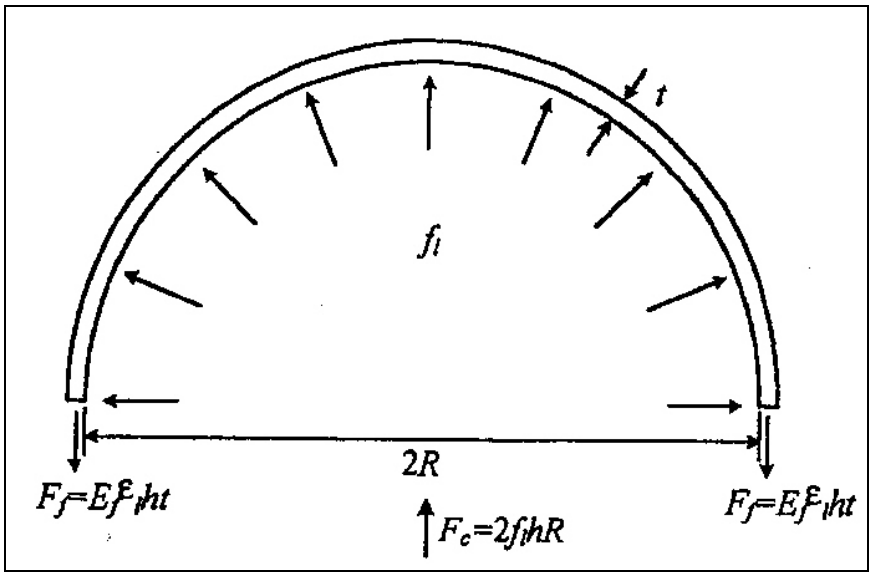

This model has two well-defined curves for the shape of the stress-strain diagram. The first branch is similar to that of shape of the stress-strain diagram of unconfined concrete, because the FRP is not fully engaged. The second branch is when the FRP is fully engaged and the stiffness is stabilizing the concrete; this branch is linear. The boundary conditions for the intersection of the first and second branch must be determined. The second branch is developed first, for simplicity.

For the development of the second branch, Equation 13 was modified from Equation 12. Equation 12 was used by Richart et al to calculate the ultimate confining stress based on concrete laterally confined with hydrostatic pressure and spiral reinforcement.

Equation 12

$$f_{cc} = f'_c + k_1 f'_l$$

where f_{cc} = confined concrete strength, f'_c = ultimate unconfined concrete stress, k_1 = confinement effectiveness coefficient and f'_l = lateral pressure. Richart et al assumed k_1 to be constant at 4.1 while others believe it to vary between 4.5 and 7.0 with an average value of 5.6. Equation 13 is as follows

Equation 13

$$f_a = f'_c + k_1 f_l$$

where f_a = calculated axial stress and f_l = lateral stress applied to the concrete by the FRP. For this model, values for k_1 were plotted at a function of the ratio between lateral stress and concrete strength (f_l/f'_c). With the use of a regression analysis, an equation for k_1 was determined with a coefficient of determination of 0.80.

Equation 14

$$k_1 = 3.5\left(\frac{f_l}{f'_c}\right)^{-0.15}$$

Substituting Equation 14 into Equation 13 will result in Equation 15. This equation will be used to calculate the stress for every point along the second branch of the stress-strain diagram.

Equation 15

$$f_a = f'_c\left[1+3.5\left(\frac{f_l}{f'_c}\right)^{0.85}\right]$$

Richart et al demonstrated that the axial strain at the maximum stress increases as a function of the lateral pressure (Toujanji, 1999, p 400). This is shown in Equation 16,

Equation 16

$$\varepsilon_{ca} = \varepsilon_o\left(1+5k_1\left(\frac{f'_l}{f'_c}\right)\right)$$

where ε_{ca} = axial strain in strength of confined concrete. If the equations used by Richart et al are substituted into the proposed equations and simplified, the axial strain for the second branch can be calculated by using Equation 17

Equation 17

$$\varepsilon_a = \varepsilon_o\left[1+k_2\left(\frac{f_a}{f'_c}-1\right)\right]$$

where ε_a = axial strain of specimens, k_2 = concrete strain enhancement coefficient and can be calculated with Equation 18, which was determined using a regression line and plotted as a function of the lateral strain with a coefficient of determination of approximately 0.85.

Equation 18

$$k_2 = 310.57\varepsilon_l + 1.90$$

Combining Equation 18 with Equation 17 will result in one last combination and simplification, resulting in the final equation (Equation 19) for determining the axial strain corresponding to the stress for the second portion of the stress-strain diagram.

Equation 19

$$\varepsilon_a = \varepsilon_o \left[1 + \left(310.57\varepsilon_l + 1.90\right)\left(\frac{f_a}{f'_c} - 1 \right) \right]$$

With the modification and combination of the equations above, the second branch of the stress-strain diagram is able to be constructed. After the second branch is constructed, the intersection point for the first and second branches must be determined. Because Richart and others initially used the yield point of steel, usually 0.002 inch/inch, to predict the stress-strain diagram of confined concrete, it was accepted by Toutanji that when the radial strain reached 0.002 inch/inch, the first and second branches intersect. Thus, the axial strain that corresponds to the radial strain of 0.002 inch/inch was used as the transition point for the two branches.

For the creation of the first branch of the stress-strain diagram, an equation, first proposed by Sargin (Toutanji, 1999) for unconfined concrete and modified by Ahmad and Shah (Toutanji, 1999), was again modified by Toutanji. Equation 20 was proposed to calculate the stress of the stress-strain diagram based on a given set of boundary conditions when the stress equals zero and the first and second branches intersect.

Equation 20

$$f_a = \frac{A\varepsilon}{1 + B\varepsilon + C\varepsilon^2}$$

where the values for the coefficients can be determined from the equations below.

Equation 21

$$A = E_{ia}$$

Equation 22

$$B = \frac{E_{ia}}{f_{ua}} - \frac{2}{\varepsilon_{ua}} + \frac{E_{ua}E_{ia}\varepsilon_{ua}}{f_{ua}^{\,2}}$$

Equation 23

$$C = \frac{1}{\varepsilon_{ua}{}^2} - \frac{E_{ua}E_{ia}}{f_{ua}{}^2}$$

where E_{ia} = initial tangent of modulus of elasticity of $f_a - \varepsilon_a$ curve, f_{ua} = axial stress between elastic and plastic regions, ε_{ua} = strain between the elastic and plastic regions in the axial direction, and E_{ua} = tangent of modulus of elasticity between elastic and plastic regions of $f_a - \varepsilon_a$ curve.

When the stress is zero, the value of E_{ia} is assumed to equal that of plain, unconfined concrete because the FRP is not engaged at this stress. Equation 24 through Equation 27 will be used to calculate the boundary constants *A*–*C*. These constants are determined using Equation 21 through Equation 23 and are used in determining the stress in Equation 20. However, these equations must be used with values in MPa. When substituted into Equation 20, the change between the first branch and the second branch smoothly transition due to the equations below.

Equation 24

$$E_{ia} = 10200\left(f'_c\right)^{\frac{1}{3}}$$

Equation 25

$$f_{ua} = f'_c\left[1 + 0.0178\left(\frac{E_l}{f'_c}\right)^{0.85}\right]$$

Equation 26

$$\varepsilon_{ua} = \varepsilon_o\left[1 + 0.0448\left(\frac{E_l}{f'_c}\right)^{0.85}\right]$$

Equation 27

$$E_{ua} = 0.3075\frac{f'_c}{\varepsilon_o}$$

Combining the above-mentioned equations for the first and second branches with values in MPa will result in the stress-strain diagram model proposed. This model's predicted stress and strain values will be compared with the actual test data.

Berthet et al (2005, 2006)

The intent of this research is to determine the factors that affect mechanical behavior of confined short columns such as confinement level, FRP properties and concrete core properties. Five different types of concretes were tested. The 28-day compressive strength varied from about 3.5 ksi to 24.5 ksi for the different concretes. The five different concretes were labeled according to their compressive strengths in MPa respectively, C20 (f'_{co} = 20 MPa (2.9 ksi)), C40 (f'_{co} = 40 MPa (5.8 ksi)), C50 (f'_{co} = 50 MPa (7.25 ksi)), C100 (f'_{co} = 100 MPa (14.5 ksi)), and C200 (f'_{co} = 200 MPa (29 ksi)). The first three concrete types had cylindrical specimens that were about 6 inches by 12 inches in shape, with the remaining two concrete types having dimensions of about 2.75 inches by 5.5 inches. The first three concrete types are to represent rehabilitated concrete structures and structural elements, while the remaining two types of concretes will represent newly constructed specimens (Berthet et al, 2004).

Subsequent to an unspecified curing time, the specimens were externally wrapped with two to 12 layers of the three different types of FRP which were impregnated with an epoxy resin. The carbon and E-glass FRPs were applied with an orientation of 0°. There were 15 plain, unconfined specimens and three of each concrete material—33 confined by carbon FRP and 15 confined by E-glass FRP.

The specimens were axially compressed at a constant rate around 0.00787 inches/minute monotonically to failure. To evaluate the axial and radial strains, a total of six LVDTs were used. They were placed about 120 apart to collect the averages. Three were used to measure the radial strains at mid-height, while three others were used to measure the axial strains. In addition to the LVDTs, strain gauges were applied at mid-height both longitudinally and transversely. The strain gauges were applied to the concrete surface for the plain specimens, but were applied to the outside of the FRP jackets of the confined specimens.

For this model, first the ultimate values for stress and strain will be calculated, then the second branch will be illustrated, finally, the first branch will be constructed. The key to using this model is to make certain that the values used throughout have metric units.

First, the ultimate confined concrete stress is determined using Equation 28,

Equation 28

$$f'_{cc} = f'_{co} + k_1 f_{lu}$$

where f'_{cc} = ultimate confined concrete strength, f'_{co} = ultimate unconfined compressive concrete strength, k_1 = efficiency ratio and was determined with regression analysis to be a constant of 3.45 when the unconfined compressive strength is between about 2.9 ksi and 7.25 ksi, while k_1 was a function of the unconfined compressive strength, calculated by Equation 29, if the unconfined compressive strength was greater than about 7.25 ksi up to about 29 ksi and f_{lu} = ultimate confinement pressure.

Equation 29

$$k_1 = \frac{9.5}{f'^{\frac{1}{4}}_{co}}$$

To determine the ultimate confinement pressure, the equilibrium equations for the cross section of an FRP-confined specimen were used under the assumption of compatibility between the concrete core and the FRP. In conjunction with Figure 2.6, the lateral confining stress can be determined by using and Equation 30.

Figure 2.6: FRP-confined concrete example cross section showing equilibrium forces

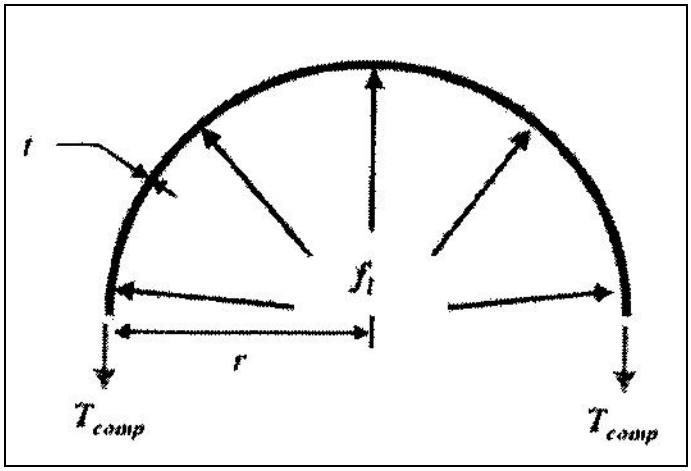

Equation 30

$$f_l = \frac{t}{r} E_{frp} \varepsilon_r$$

where f_l = lateral confining stress, t and r are the thickness of the FRP and radius of the concrete core, respectively, E_{frp} = modulus of elasticity of the FRP as provided by the manufacturer, ε_r = radial strain. Since the ultimate confining stress is needed to calculate

the ultimate confined stress, Equation 31 is a modification of Equation 30 in which the ultimate strain in the FRP jacket is used as provided by the manufacturer;

Equation 31

$$f_{lu} = \frac{t}{r} E_{frp} \varepsilon_{fu}$$

where f_{lu} = ultimate lateral confining stress, ε_{fu} = ultimate radial strain as provided by the manufacturer and all other variables remain the same. Substituting Equation 31 into Equation 28 with the appropriate k_1 value will result in Equation 32.

Equation 32

$$f'_{cc} = f'_{co} + k_1 \frac{t}{r} E_{frp} \varepsilon_{fu}$$

Once the ultimate confined stress is determined, the ultimate strain needs to be determined. The relationship between the axial and radial strain values indicates two distinct branches: a "pseudo-elastic" branch and a branch which depicts the yield point of the specimen. This change in slope corresponds to the transformation from pseudo-elastic to pseudo-plastic. This is associated with the unconfined, plain compressive axial strain, which is about 0.002 inch/inch.

To define the ultimate strain, the relationship between the confining pressure and the transverse strain must be defined as in Equation 33, along with the expression for the strain ratio shown below in Equation 34;

Equation 33

$$E_l = \frac{\Delta f_l}{\Delta \varepsilon_r} = \frac{t}{r} E_{frp}$$

Equation 34

$$\gamma = \frac{1}{\sqrt{2}} \left(\frac{E_l}{f'^{\,2}_{co}} \right)^{-\frac{2}{3}}$$

where E_l = confinement modulus of elasticity, Δf_l = change in confining stress, $\Delta \varepsilon_r$ = change in radial strain, t and r are the thickness of the FRP and the radius of the concrete core, respectively, E_{frp} = Young's modulus of confinement of the FRP, γ = plastic strain ratio, and f'_{co} = unconfined compressive strength of concrete.

With the above equations defined, the ultimate strain can now be calculated using Equation 35

Equation 35

$$\varepsilon_{au} = \varepsilon_{ao} + \sqrt{2}\left(\frac{E_l}{f'^{\,2}_{co}}\right)^{\frac{2}{3}}\left(\varepsilon_{fu} - \nu_c\varepsilon_{ao}\right)$$

where ε_{au} = ultimate axial strain of confined concrete, ε_{ao} = ultimate axial strain of unconfined concrete (typically taken to be 0.002 inch/inch), ε_{fu} = ultimate FRP strain as provided by the manufacturer, and ν_c = Poison's ratio (typically taken to be 0.2). Plotting the ultimate stress and ultimate strain should result in a single point with which the second branch should end.

The second branch of the stress-strain diagram for confined concrete is linear. For calculating the second branch, the slope of this linear relationship was determined with a best fit linear regression with a 99% coefficient of determination to be determined by using Equation 36

Equation 36

$$\theta_r = 2.73E_l - 163$$

where θ_r = slope of the pseudo-plastic branch which corresponds to the change in stress with the change in plastic strain.

Since this model is constructed from end to beginning, the slope of the line for the second branch as calculated by Equation 36 will be used to determine the intersection point for the first and second branches. Now that the slope is defined, the transition point must be defined. The transition point is where the second branch will smoothly join together the first and second branches of the stress-strain diagram. First, the transition stress value will be calculated using Equation 37

Equation 37

$$f'_{cp} = f'_{cc} - \theta_r\left(\varepsilon_{fu} - \varepsilon_{rp}\right)$$

where f'_{cp} = reference plastic stress or the transition stress where the first and second branch intersect and ε_{rp} = radial strain at the intersection between the first and second branch; this value will be taken as 0.002 inch/inch. Then, the transition stress is used with Equation 38

Equation 38

$$f'_c = f'_{cp} + \theta_r \left(\varepsilon_r - \varepsilon_{rp} \right)$$

where $\varepsilon_r \geq \varepsilon_{rp}$ so that every value of stress for the second branch can be calculated for every value of radial strain greater than that of ε_{rp}. Establishing a connection between the radial strain and the axial strain will allow for the equations above to be applied when the axial strain is known. The relationships are as follows:

Equation 39

$$\varepsilon_r = \nu_c \varepsilon_a$$

Equation 40

$$\varepsilon_r = \nu_c \varepsilon_{ao} + \gamma \left(\varepsilon_a - \varepsilon_{ao} \right)$$

where Equation 39 would be used when $\varepsilon_a \leq \varepsilon_{ao}$ and Equation 40 would be for when $\varepsilon_a \geq \varepsilon_{ao}$ and where Equation 34, above, would define γ. With the equations above, the stress corresponding to the axial strain can be determined with a few simple substitutions. This will result in Equation 41

Equation 41

$$f'_c = f'_{cp} + \theta_r \left[\left(\nu_c - \gamma \right) \varepsilon_{ao} - \varepsilon_{rp} \right] + \theta_r \gamma \varepsilon_a$$

when $\varepsilon_a \geq \varepsilon_{ap}$ where ε_{ap} is found using Equation 42

Equation 42

$$\varepsilon_{ap} = \varepsilon_{ao} + \frac{\varepsilon_{rp} - \varepsilon_{ro}}{\gamma}$$

where ε_{ap} = axial plastic strain corresponding to ε_{rp}, ε_{ao} = unconfined compressive strain (typically 0.002 inch/inch), and ε_{ro} = radial strain of unconfined concrete which can be determined using Poisson's ratio (assuming that the value for Poisson's ratio is 0.2 as is customarily agreed upon as standard) and ε_{ao}.

Applying Equation 41 for strain values greater than or equal to that which are found using Equation 42 will result in the displaying of the second branch of the stress-strain diagram where axial strain is calculated based on the corresponding radial strain. Now, the first branch must be constructed with the second branch transitioning smoothly.

This will be done with Equation 43, first proposed by Ahmad and Shah, and more recently modified and presented by Toutanji.

Equation 43

$$f'_c(\varepsilon) = \frac{A\varepsilon}{1 + B\varepsilon + C\varepsilon^2}$$

where the coefficients A, B, and C can be determined by Equation 44, Equation 45, and Equation 46 and where E^*_r represents the transverse equivalent modulus of the multi-material of the FRP and the concrete core, which can be determined using Equation 47.

Equation 44

$$A = E^*_r$$

Equation 45

$$B = \frac{E^*_r}{f'_{cp}} - \frac{2}{\varepsilon_{rp}} + \theta_r \frac{E^*_r \varepsilon_{rp}}{f'^{\,2}_{cp}}$$

Equation 46

$$C = \frac{1}{\varepsilon_{rp}} - \theta_r \frac{E^*_r}{f'^{\,2}_{cp}}$$

Equation 47

$$E^*_r = \frac{E_c}{\nu_c}\left[1 + \frac{E_l}{E_c}(1 - \nu_c)\right]$$

For Equation 43 to be used with axial strains instead of radial strains, there must be an alteration where ε is replaced by ε_a. This will result in changed boundary conditions and a slight change in the coefficients defined above, where E^*_r will be replaced with E^*_a which is defined as Equation 48

Equation 48

$$E^*_a = E_c \frac{E_c + (1 - \nu_c)E_l}{E_c + (1 - \nu_c - 2\nu_c^2)E_l}$$

where E^*_a represents the equivalent elastic modulus. The equation above, in conjunction with the translation between the axial strain corresponding to the radial strain ε_{rp}, can be used to substitute into Equation 43, which will result in Equation 49.

Equation 49

$$f'_c = \frac{E_a^* \varepsilon_a}{1 + \left(\frac{E_a^*}{f'^{\,2}_{cp}} - \frac{2}{\varepsilon_{ap}} + \frac{\theta_r E_a^* \varepsilon_{ap}}{f'^{\,2}_{cp}} \right) \varepsilon_a + \left(\frac{1}{\varepsilon_{ap}^{\,2}} - \frac{\theta_r E_a^*}{f'^{\,2}_{cp}} \right) \varepsilon_a^{\,2}}$$

Combining the stress values from Equation 49 partnered with the axial strain up to ε_{ap} along with the stress values obtained from Equation 41 together with the strains greater than ε_{ap} will result in the complete stress-strain diagram. Since these equations are only valid in metric units, once the stress is determined in MPa, it will be converted to ksi to allow for comparison with the experimental test data.

Teng & Lam (2003, 2004)

Results from 76 plain, FRP-confined concrete cylinder specimens were obtained from open literature. The diameters ranged from about 4 inches to 8 inches with unconfined compressive strengths that ranged from about 3.8 ksi to 8 ksi. Only specimens that failed due to ruptured FRP from hoop tension were analyzed. Failure of FRP-confined concrete occurs when the hoop rupture strength of the concrete is reached in the FRP. The confining pressure can be determined by Equation 50 and Equation 51

Equation 50

$$\sigma_r = \frac{\sigma_h t}{R} = \frac{2\sigma_h t}{d}$$

Equation 51

$$\sigma_h = E_{frp} \varepsilon_h$$

where σ_h = hoop stress, E_{frp} = modulus of elasticity, ε_h = hoop strain of the FRP as a function of FRP thickness and the radius of the confined concrete core, t and R or d, respectively (Teng and Lam, 2004). Since the maximum hoop strain at rupture, as provided by the manufacturer, is often higher than that of actual confined concrete specimens, a comparison of this information was made. It was determined that a ratio for actual confinement as represented by $f_{l,a}$ and f'_{co} would be necessary to determine the actual hoop rupture strain. This value was determined to be 0.63 for all 76 specimens, even though the concrete strength and confinement type varied. Table 2.3 shows the

average ratio values based on the different confinement types. Equation 52 represents the actual maximum confining pressure,

Equation 52

$$f_{l,a} = \frac{2E_{frp}t\varepsilon_{h,rup}}{d}$$

where $f_{l,a}$ = actual confining pressure and $\varepsilon_{h,rup}$ = hoop strain at rupture.

Table 2.3: Average hoop rupture strain ratios

Type of Fiber	**No. of Specimens**	**FRP material ultimate tensile strain ε_{frp} from coupon tests**		**Ratio of hoop rupture strain to FRP material ultimate tensile strain $\varepsilon_{h,rup}/\varepsilon_{frp}$ (%)**	
		Average	*S.D.*	*Average*	*S.D.*
CFRP	52	0.0148	0.0015	58.6	15.3
High Modulus CFRP	8	0.0045	0.0027	78.8	16.8
AFRP	7	0.0223	0.0068	85.1	9.5
GFRP	9	0.0280	0.0136	62.4	36.4
Total	76	0.0160	0.0080	63.2	20.5

The stress-strain diagram for FRP-confined concrete shows a bilinear response, while that of actively confined concrete shows a softening branch. This is in response to the increase in confining pressure with the increase in axial stress, when the cylinder is confined with FRP; however, with active pressure, the lateral confining pressure is constant throughout the test even as the axial load increases. For the concrete to behave with the bilinear response there must first be sufficient confinement or the standards for the minimum confinement level must be set. For circular specimens, if the actual confinement ratio $f_{l,a}/f'_{co} \geq 0.07$, it has been determined that adequate confinement has been provided; thus the stress-strain diagram will have a bilinear response. The overall consensus is that the initial branch of the stress-strain diagram is one that tends toward parabolic and is similar to the stress-strain diagram for unconfined concrete, but takes into consideration the fact that the FRP becomes engaged once microcracking occurs, and is linear for the second portion.

There are two divisions for the models that exist for confined concrete: design-oriented and analysis-oriented. Design-oriented models "are presented in closed-form

expressions" while analysis-oriented models are constructed based on "an incremental iterative numerical procedure" (Teng & Lam, 2004). To be considered a design-oriented model, there has to be some ease to the equations and processes which will easily allow for the direct computation by hand or by using spreadsheets. Analysis-oriented models are those that are too cumbersome to do with hand calculations, due to the great number of iterations required. Two typical processes are used in the development of FRP-confined concrete models: the general expression proposed by Sargin in 1971 and the four parameter stress-strain diagram proposed by Richard and Abbot in 1975.

The design-oriented models are based on Sargin's general expression, which is given by Equation 53 (Teng and Lam, 2004).

Equation 53

$$\frac{\sigma_c}{f'_{co}} = \frac{\frac{A\varepsilon_c}{\varepsilon_{co}} + (D-1)\left(\frac{\varepsilon_c}{\varepsilon_{co}}\right)^2}{1+(A-2)\left(\frac{\varepsilon_c}{\varepsilon_{co}}\right)+D\left(\frac{\varepsilon_c}{\varepsilon_{co}}\right)^2}$$

In Equation 53 A and D are constants that control the initial slope and descending path of the stress-strain curve, respectively. Among the models that use Sargin's general expression, some use Equation 53 while others use the modified version, Equation 54, where $A = 2$ and $D = 0$ and $\varepsilon_{co} = 0.002$ inch/inch.

Equation 54

$$\frac{\sigma_c}{f'_{co}} = \frac{\varepsilon_c}{\varepsilon_{co}}\left(2-\frac{\varepsilon_c}{\varepsilon_{co}}\right)$$

Some of the models produce bilinear predictions while others are predicted linearly. The authors of the different models can be found in the review of existing models provided by Teng and Lam (2004). Some generate a descending as well as an ascending portion while others only predict an ascending portion.

Models, based on the four parameters by Richard and Abbot, were proposed to determine the elastic-plastic behavior (Teng & Lam, 2004). These four parameters for determining the stress and strain are established in Equation 55

Equation 55

$$\sigma = \frac{\left(E_1 - E_2\right)}{\left\{1 + \left|\frac{\left(E_1 - E_2\right)\varepsilon}{f_o}\right|^n\right\}^{1/n}} + E_2\varepsilon$$

where f_o = reference stress, and E_1 = initial modulus, E_2 = plastic modulus and n = shape parameter used to control the transition between the first branch and second branch of the stress-strain diagram. Figure 2.7 graphically represents Equation 55 mentioned above. The benefit to this method is that only one equation is needed to get the complete bilinear stress-strain relationship.

Figure 2.7: Richard and Abbot model explaining equation above

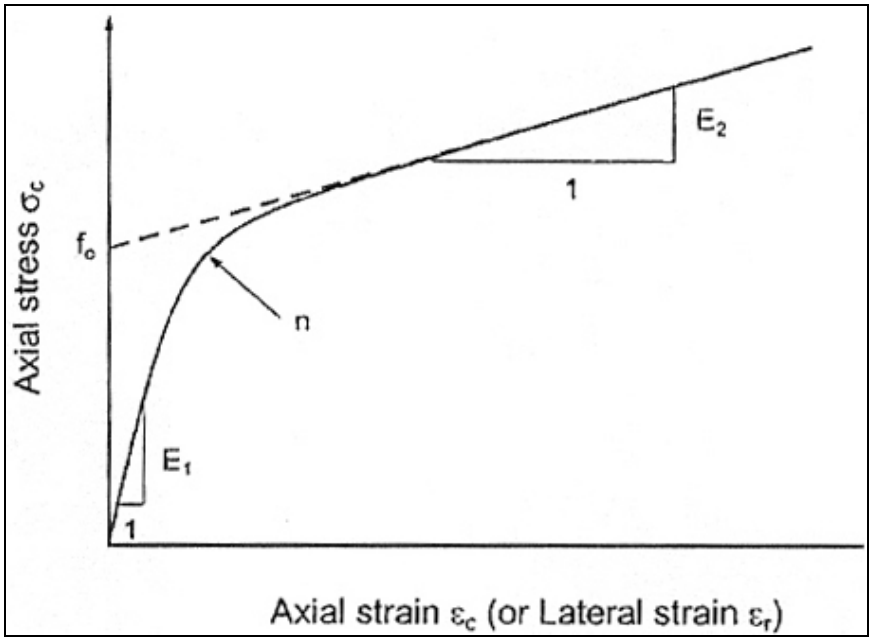

The model by Lam and Teng (2003) that has been proposed has a parabolic first section with the initial modulus being the same as that of the unconfined concrete's initial modulus. The linear second segment has a modulus that correlates to a reference stress that is equal to that of the unconfined compressive stress. The linear portion meets the parabolic portion at a certain strain, slightly higher than that of the ultimate unconfined compressive strain. Figure 2.8 illustrates the foundation for the Lam and Teng model and how the variables are determined.

Figure 2.8: Explanation of variables proposed by Lam & Teng

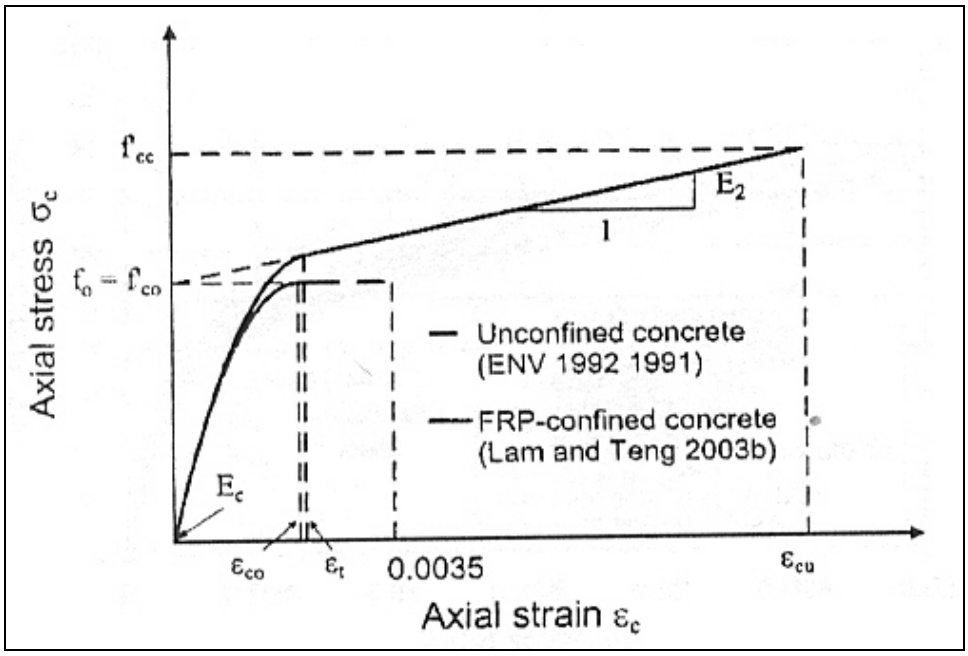

Using the figure above, the model is constructed using Equation 56 when the concrete strain varies from zero up to the transition strain ($0 \le \varepsilon_c \le \varepsilon_t$), and can be created from the transition strain up to the ultimate strain ($\varepsilon_t \le \varepsilon_c \le \varepsilon_{cu}$) with Equation 57, where the transition strain is determined using Equation 58.

Equation 56

$$\sigma_c = E_c\varepsilon_c - \frac{\left(E_c - E_2\right)^2}{4f_o}\varepsilon_c^{\,2}$$

Equation 57

$$\sigma_c = f_o + E_2\varepsilon_c$$

Equation 58

$$\varepsilon_t = \frac{2f_o}{(E_c - E_2)}$$

where f_o = intercept of the stress axis by the linear second portion, E_2 = slope of the linear second branch which can be determined by using Equation 59

Equation 59

$$E_2 = \frac{f'_{cc} - f_o}{\varepsilon_{cu}}$$

where f'_{cc} = compressive strength of confined concrete.

Since Lam and Teng believe that during the construction of the stress-strain diagram, the effects of the jacket stiffness need to be considered. With the stiffness of the FRP jackets taken into consideration, the normalized ultimate strain value can be determined using Equation 60

Equation 60

$$\frac{\varepsilon_{cu}}{\varepsilon_{co}} = 1.75 + 12\left(\frac{f_{l,a}}{f'_{co}}\right)\left(\frac{\varepsilon_{h,rup}}{\varepsilon_{co}}\right)^{0.45}$$

where the value for ε_{co} is assumed to be 0.002 inch/inch based on all the available test data from the studies of the open literature. The normalized compressive strength of confined concrete is related to the nominal confinement ratio as given by Equation 61

Equation 61

$$\frac{f'_{cc}}{f'_{co}} = 1 + 2\frac{f_l}{f'_{co}}$$

and is thoroughly discussed in a different published paper. However, when the actual confinement ratio is used, Equation 61 becomes that which is illustrated by Equation 62

Equation 62

$$\frac{f'_{cc}}{f'_{co}} = 1 + 3.3\frac{f_{l,a}}{f'_{co}}$$

where the confinement ratio $f_{l,a}/f'_{co} \geq 0.07$ to ensure that sufficient strength enhancement will be available.

The value for f_o for this model was determined based on available data and tests conducted by the authors. The average ratio of $f_{l,a}/f'_{co}$ was determined to be 1.09 with a standard deviation of 0.13; thus from the analysis, the value for f_o was determined to be nearly f'_{co} and will be considered f'_{co} for simplicity.

For ease of analysis and construction of the stress-strain diagram, Equation 63 will replace Equation 60. This takes into account the fact that the actual rupture strain will not be required to be known.

Equation 63

$$\frac{\varepsilon_{cu}}{\varepsilon_{co}} = 1.75 + 5.53\left(\frac{f_{l,a}}{f'_{co}}\right)\left(\frac{\varepsilon_{frp}}{\varepsilon_{co}}\right)^{0.45}$$

When CFRP is used as the confining material and the FRP efficiency factor of 0.586 is used from Table 2.3 to adjust the manufacture's listed value for the rupture strain of the FRP, the use of Equation 63 will result in the normalized ultimate strain value without the actual hoop rupture strain being known. The authors note that this efficiency factor has quite a wide range, and thus a small sample of confined cylinders should be tested to determine a safe and cost-effective amount of FRP that should be applied. The authors also propose that a standard should be set so that manufacturers can provide this information in comparison to plain cylinders, and if this information is not provided by the manufacturer, then the client should conduct the tests.

Analysis-oriented models are based on an incremental iterative numeric method which accounts for the interaction between the concrete core and the confining FRP. This method is extensive and thus does not lend to easy hand or spreadsheet computations; however, it can be easily accomplished in a computer as a non-linear finite element analysis. These models make the assumption that the axial stress and strain of FRP-confined concrete at a given lateral strain are the same as those of the concrete with the same properties actively confined to a pressure that would be equivalent to the pressure that an FRP jacket would apply. This assumption has not been tested, but has been accepted (Teng & Lam, 2004).

CHAPTER 3 - Experimental Program

The experimental program required construction of the specimens, application of the confinement, set-up of the test, and administration of tests under various loading conditions.

Construction of the specimens included designing the type of concrete with the desired compressive strength, and placing the order, casting the concrete for each

cylindrical specimen, curing the specimens under controlled conditions and testing the samples for unconfined compressive strength.

Application of the strain gauges included, specimen cleaning and the pertinent preparations that were required prior to applying the strain gauges on the specimens. Attachment of the confinement included measuring and cutting of the FRP sheets, as well as mixing of the two-part epoxy and impregnating the FRP sheets and affixing them to the specimens, ensuring a complete contact throughout the application process.

Set-up of each test depended on type of the test to be conducted on the specimen in terms of the type of loading protocol, maximum load, and loading rate. This included programming of the testing equipment and testing of the program functionality and administration of the tests. Due to insufficiency of the capacity of the existing actuators and a need for more compressive force to load some of the samples to their failure, a system was fabricated that works similar to a nutcracker, shown in Figure 3.1, was constructed to achieve the necessary force. Once this device was built, the tests were set-up and coordinated again. During both rounds of testing the data was carefully collected, analyzed, and compared against the representative models proposed by the aforesaid researchers for the behavior of the tested specimens.

Figure 3.1: Nutcracker-like device used to multiply force applied to specimens

Materials

For the experimental program, four concrete cylinders with the standard size of 6 inches by 12 inches, diameter and height, respectively, were cast. The concrete used for construction of the specimens was supposed to have a 28-day compressive strength of 2.5 ksi, ordered from a local concrete plant. This strength was chosen because of the known limitations of the testing equipment. The concrete was batched at the concrete plant and trucked to the laboratory where it was placed in the cylinders. To have a realistic value for the compressive strength of the plain, unconfined concrete used for construction of the specimens, four concrete cylinders with dimensions of 4 inches by 8 inches, were tested and the average 28-day compressive strength was determined to be about 5.4 ksi. All of the specimens were capped with sulfur to ensure a level surface. The specimens that were intended to be confined had the lip of the sulfur caps ground down for a smooth surface when applying the confinement.

Each specimen had a total of five strain gauges applied to the surface of the concrete. The strain gauges were two inches long with a 120Ω resistance. Due to time constraints, some of the gauges had to have the wires soldered on immediately prior to application of the FRP, while others were pre-soldered from the manufacturer with the leads and wires already attached. The data collection system used was the Mega Dac, a 200-channel logger, connected to the computer to collect the data from the data logger at an approximate collection rate of 2.5 seconds.

CFRP sheets were used as the confinement. The high-strength carbon fiber used was unidirectional and had properties as seen in Table 3.1 below. A two-part epoxy resin, V-Wrap 776 Resin/Filler Component A and Component B, was used to impregnate the CFRP. Each cylinder was wrapped continuously, with the orientation of the fibers in the 0° direction, with two layers of the impregnated CFRP. The ratio of resin to hardener was 3:1 which was mixed in a graduated container by hand until there was a uniform color between the resin and hardener. To ensure that there was a proper amount of FRP to keep the wrap fully engaged during testing, the length of the CFRP was extended by approximately 25% of the circumference, which equates to about 4 inches. The wrapped specimens were left at room temperature to cure for one day before the first round of tests

was conducted. The epoxy properties at failure according to the manufacturer are indicated by Table 3.2.

Table 3.1: CFRP properties as provided by the manufacturer

V-Wrap C100	VSL Strengthening Products (manufacturer)
Nominal Thickness	0.0065" per ply
Ultimate Tensile Strength	550 ksi (per unit width 3.57k/in/ply)
Tensile Modulus	33,000 ksi (per unit width 215k/in/ply)
Ultimate Rupture Strain	1.67%

Table 3.2: Epoxy properties at time of failure as provided by the manufacture

Tensile Strength	4.5 ksi
Flexural Modulus	575 ksi
Elongation	2.5 %

Instrumentation

Strain Gauge Location and Application

Three strain gauges were longitudinally, affixed on the surface of the specimen at the mid-height, and120° apart radially. The remaining two strain gauges were radial gauges also located at mid-height about 180° away from each other. The measurements from these gauges were used to calculate the average strain within the two-inch central portion of the cylindrical specimens. Figure 3.2 shows the typical placement of the longitudinal and radial strain gauges on the specimens.

Figure 3.2: Typical gauge placement on specimens

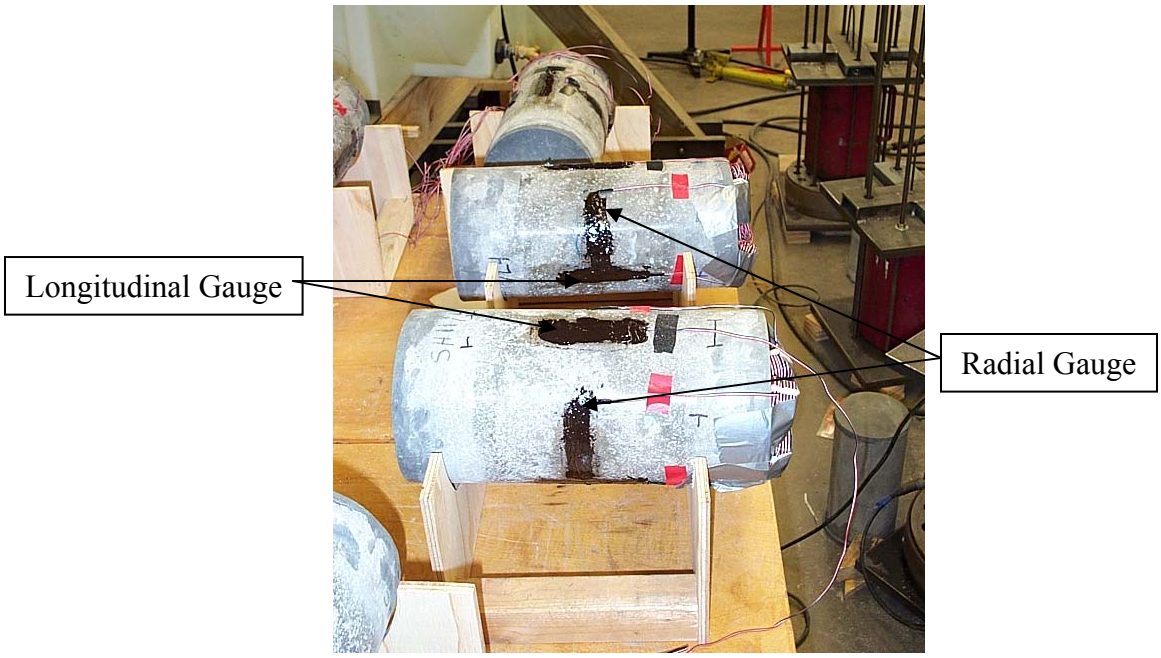

FRP Application

Since the epoxy cure time was listed as six hours, the FRP was applied to the specimens one day prior to testing, to ensure adequate curing time. The process of applying the FRP and epoxy was as follows. A carbon-fiber sheet was measured and cut to the height (12 inches) and twice the circumference plus the 25% overlap (about 44 inches). Two strips 2 inches wide and about 44 inches long were also cut for each specimen. The resin and hardener were mixed until uniform in color. The two-part epoxy was brushed onto one side of the CFRP sheet then a roller was used to ensure total impregnation. This sheet was rolled onto the cylinder keeping as much tension in the sheet as possible to ensure that the epoxy impregnated sheet was in full contact with the specimen and with the first layer. The 2-inche wide strips were then impregnated with the epoxy. These strips were applied to the top and bottom of the specimens to force the failure to occur in the central region of the specimens.

Specimen Testing Setup

Figure 3.3 shows the instrumentation and set-up for a typical specimen during the first round of testing. A hydraulic testing machine was used to apply load to each specimen. A 200-kip load cell was attached to the actuator to measure the load that was

applied to the specimen. A plate was attached to the load cell to protect the load cell during loading and provide a level surface. A Linear Variable Displacement Transducer (LVDT) was installed to measure the amount of axial displacement during the testing process. This was the main LVDT which was used to control the testing apparatus when testing in displacement control and for initial set up when testing in force control during the first round of testing. Two smaller LVDTs were placed at the front (near) and back (far) side of the cylinder to measure the global strain of the cylinder. Four potentiometers were placed on the four corners of the plate extending past the cylinder. The potentiometers were also used to measure the global strain in the cylinder.

Figure 3.3: Loading and typical apparatus set up and instrumentation of specimens

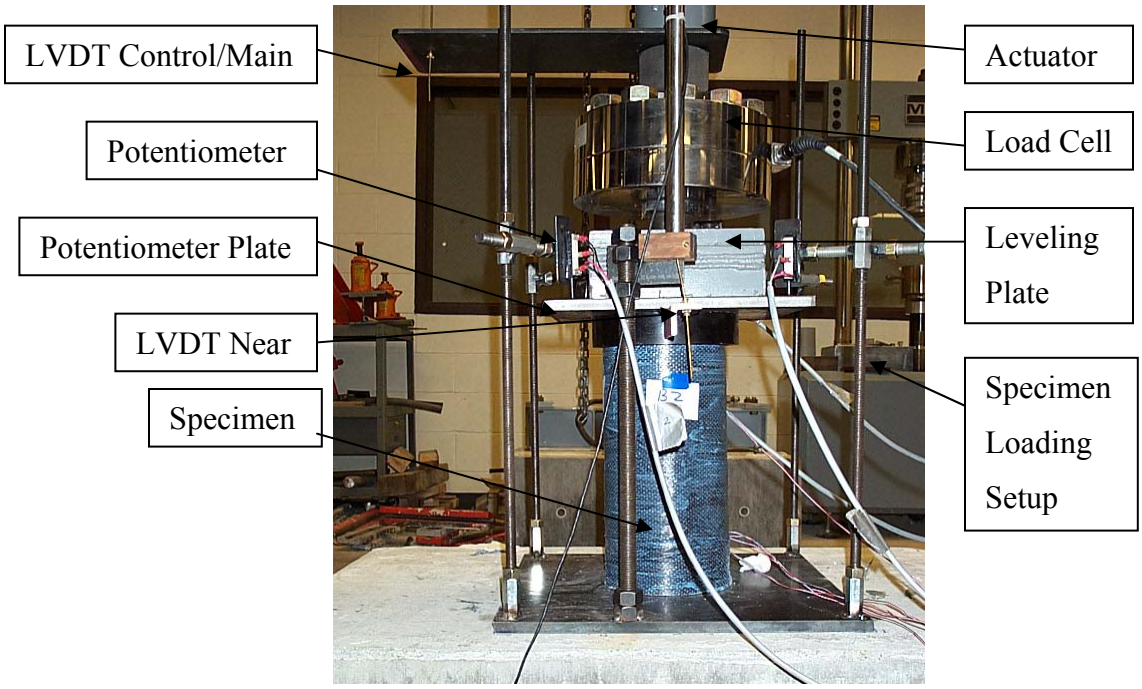

The figure above shows the set-up of the specimens during the first attempt to load the specimens to failure. Figure 3.4 shows the nutcracker-like device and dummy cylinder similar to how the new testing set-up will be in the future, excluding the location and placement of the data collection devices, such as the potentiometers. This device allowed the specimens to be pushed to failure.

Figure 3.4: Device constructed to allow failure of the specimens

For the second round of testing, the main LVDT was used to control the actuator for the entirety of the tests, since all were conducted in displacement-control mode. The LVDT was mounted to the actuator to reduce some of the fluctuation that had occurred during previous of testing and initial set-up for the second round of testing. The near and far LVDTs were not part of the testing set-up and data collection process. Testing set-up for round two of test can be seen in Figure 3.5 below.

Figure 3.5: Typical testing set up for the second round of tests

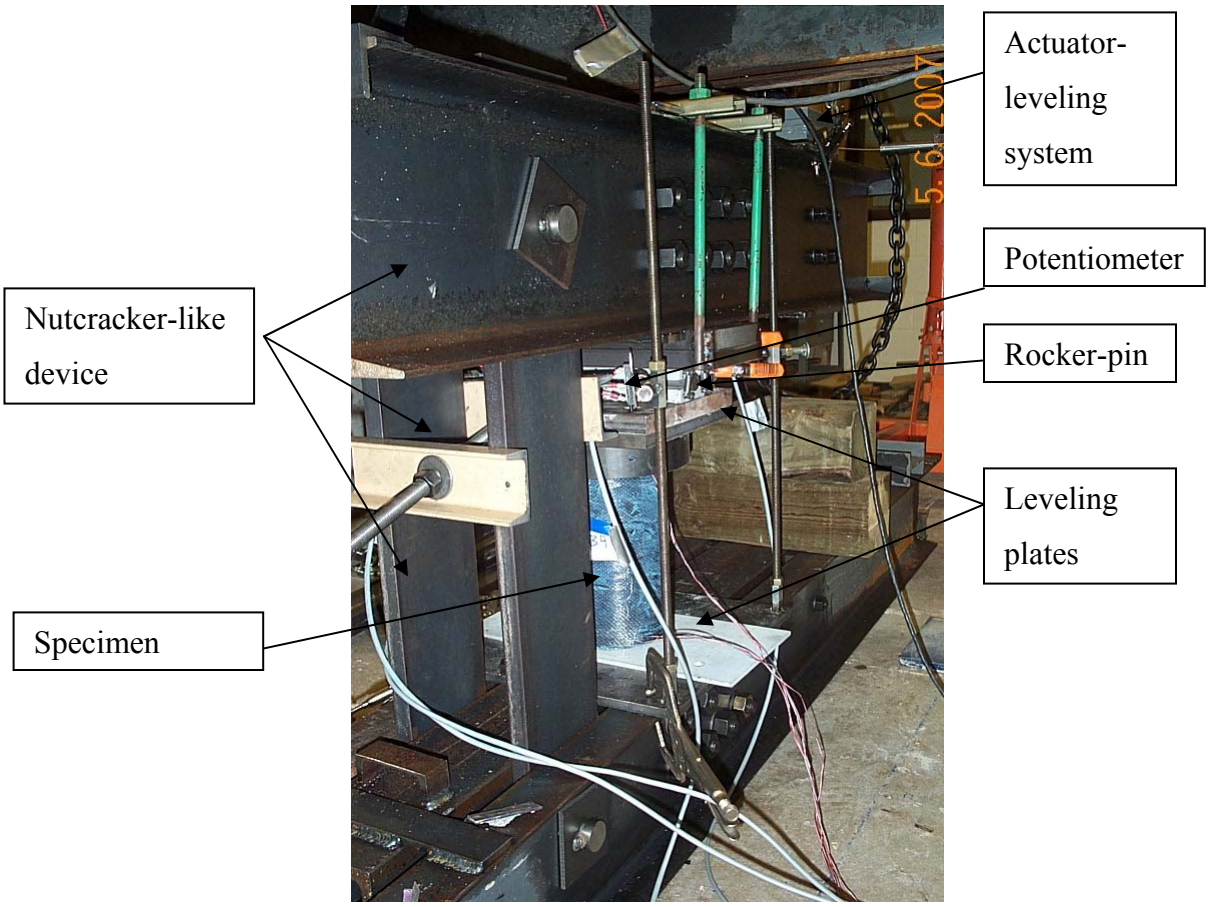

System Control

The machine used to control the loading rate was the Multipurpose Testware System (MTS). The MTS can be operated in two modes: displacement control mode and force control mode. In displacement control mode the rate of strain is constant throughout the testing, while in force control mode, the rate of stress is constant throughout the duration of the tests. During the initial round of testing, two of the tests were conducted in force control mode and the remaining two tests were conducted in displacement control mode. The actuator used in the test had a maximum capacity of 150 kips. The LVDT was used as the displacement feedback to the MTS control system. The concrete had a higher strength than expected, resulting in the need for the nutcracker-like device. Due to this device being used to repeat the tests that were previously conducted, all tests using this apparatus were only conducted in displacement-control mode to ensure personal safety as well as equipment safety.

Testing

Four standard four-inch cylinders, which were cast at the same time as the six-inch cylinders, were prepared for compressive testing. These cylinders were used to determine the unconfined compressive strength of the concrete. The test on the four-inch samples was conducted immediately prior to the testing of the confined specimens for the first attempt. It was the intent to monotonically load the specimens at a constant rate, either rate of strain or rate of stress to failure. However, due to the lack of available force during the first round of tests, the specimens were loaded to the maximum allowable load as provided by the actuator. Then the specimens were unloaded and three of the four specimens were held at a targeted sustained load of 42 kips, with a variance of approximately 2%, until the second round of tests could be conducted. The device that was used to deliver the sustained load can be seen in Figure 3.6 below. During the second round of testing, the specimens were monotonically loaded at a constant rate of strain until failure or until personal safety or equipment safety was thought to be in jeopardy.

Figure 3.6: Sustained load device & set-up

First Attempt

For specimens tested in force control, the loading pattern was such that the actuator was programmed by the MTS to apply a load at a constant load rate. For the

specimens tested in displacement control, the load was applied at a constant displacement rate. The constant rate for the load for the force controlled specimens was 60 kips/minute and the rate for the displacement controlled specimens was 0.0068 inches/minute. These values were determined based on the ASTM standard C-469 for compression testing of concrete or 35 psi/s. Because the capacity of the actuator was only 150 kips and the concrete had an average compressive strength of 5.4 ksi, the test specimens were not able to be loaded up to the peak value for unconfined concrete, to transition into the plastic branch of the stress-strain diagram, and finally to fail.

Second Attempt

Due to the apparatus being used for the testing of the specimens, and being alarmed about the safety of the testing crew and the testing equipment, no tests were conducted in the force-control mode. All the specimens tested with the nutcracker-like device were tested in displacement-control. The load was applied so that a constant displacement rate of 0.0167 inches/minute was provided. These values were determined based on the results from the previous tests in addition to the results from other researchers. This value was within the range, on the high end, of the displacement rates of other researchers. Loading at this rate would ensure a compressive failure instead of a creep failure.

CHAPTER 4 - Experimental Results

Due to there being a slight lack of available force from the testing machine, there was a period of about 75 days between the first round and the second round of tests. This was because it took that long before the device was finally constructed allowing for the specimens to be loaded to failure. During this time, three of the four specimens were held under a sustained load after the initial testing. The fourth specimen had no load applied after the initial testing. The sustained load was applied to assist a Ph. D. research student. Information was needed on CFRP wrapped specimens that had been initially loaded, to determine if there is a difference in the behavior and shape of the stress-strain diagram.

The experimental data results of both rounds of tests were collected and compiled. These results were analyzed and adjusted to show the stress-strain diagrams of the experimental data. The test data were then used to construct the expected stress-strain curves based on the equations from the existing models with which the experimental data is being compared and which it is intended to validate.

Round One

In this section of the paper the test data from the first round of testing will be compared with the each of the five models. All the strain data was recorded along with the load and displacement. This information was used to construct the stress-strain curves and compare them with the models proposed by Popovics, Mansur et al, Toutanji, Berthet et al and Teng and Lam. Conclusions about these models' validity will be made in the next chapter.

Popovics

The idea that there was a difference in the shape of the stress-strain diagram if the specimen was loaded with either a constant stress or constant strain was to be investigated for confined concrete, even though this model was based on unconfined, plain concrete. In comparing the experimental data, it can be seen in Figure 4.1 that when the strain is measured in the central portion of the specimen, the shapes of the ascending branch of the stress-strain diagrams for the two different loading patterns and rates were nearly identical. These test results are contrary to the idea behind the purpose for Popovics' model. The model proposed by Popovics indicates that when loading at a constant rate of stress compared to loading at a constant rate of strain, the initial modulus of elasticity for the constant rate of stress is higher than that of the modulus for the constant rate of strain as can be seen in Figure 4.2 below.

Figure 4.1: Stress-strain diagram for specimens with constant stress & strain rates

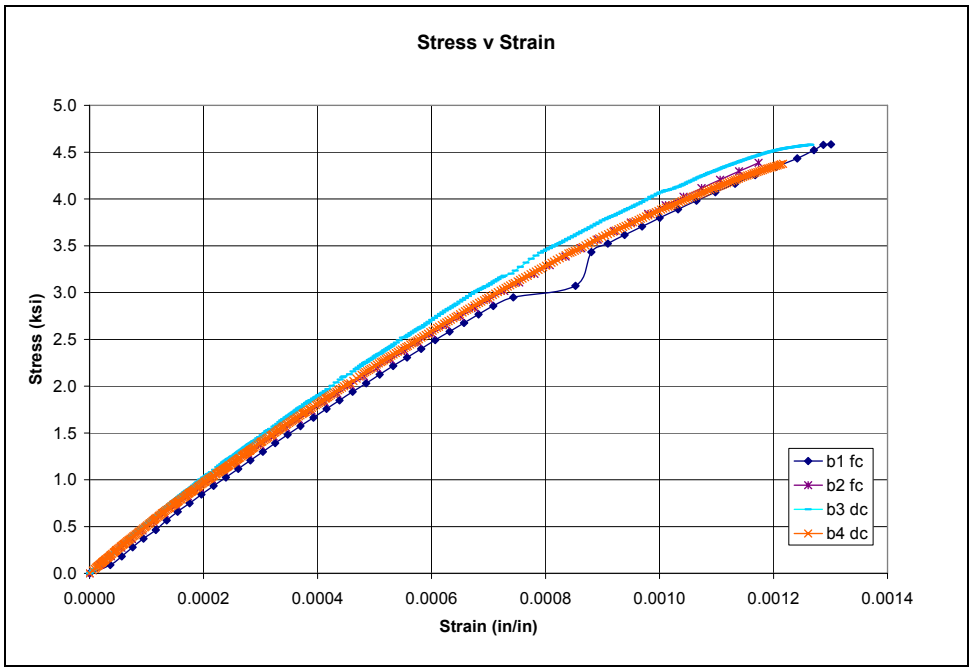

Figure 4.2: Stress-strain diagram with constant stress or constant strain applied

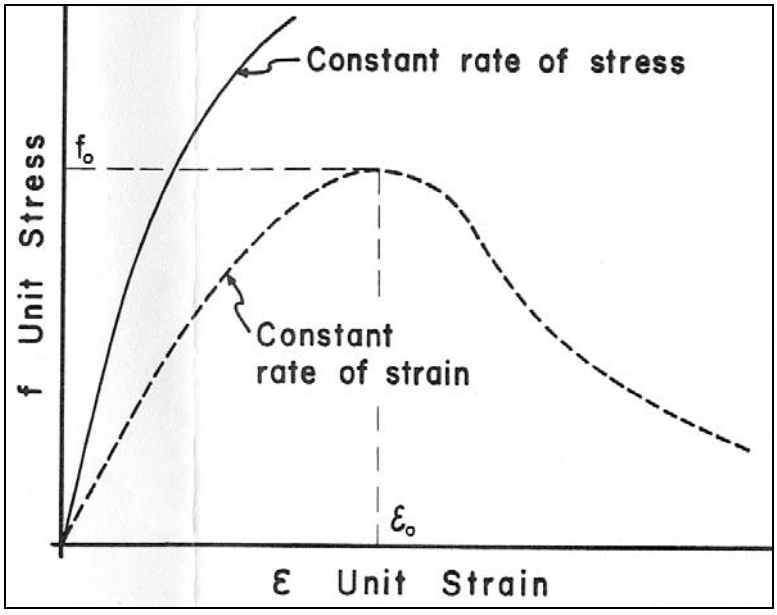

Calculating the strains from the measurements taken from the potentiometers, which were set up to measure deformation over the entire length of the test specimens, results in a difference in the stress-strain diagram that slightly resembles the stress-strain diagram as proposed by Popovics above. Figure 4.3 shows the results from the experimental data where the strain was measured globally, and compares shape of the

stress-strain diagram of loading with a constant stress compared to a constant strain rate. From the figure, it can be seen that there are two distinct branches; however, each branch has one specimen from each category: constant rate of stress and constant rate of strain. Thus, the loading pattern (constant stress as opposed to constant strain) appears to have little relevance in the shape of the stress-strain diagram.

Figure 4.3: Stress-strain curves for constant stress & strain rates measured globally

The LVDTs that were at the front and back of the specimens, resulted in there being inconclusive findings. The intent was to compare the potentiometer measurements with the LVDT measurements to see if a correlation between the two could be determined and how this information compared with the theory that constant stress rates versus constant strain rates changed the shape of the stress-strain diagram. The possible reason for inconclusive results could be related to the manner in which the LVDT was attached to the actuator that controlled the rate of load applied.

Since there is no apparent evidence that there is a difference in the stress-strain diagram when comparing specimens loaded at a constant strain versus specimens loaded at a constant stress, the equations above provided by Popovics do not need to be compared with this data set, but for evaluation of the model, the two specimens that were loaded in displacement control were compared with the model and the results can be seen in Figure 4.4 and Figure 4.5 below. In both cases, the test data splits the two predictions.

When only the ultimate stress is known, the model is conservative, but when both the ultimate stress and the ultimate strain are known, the stress for any given strain is overpredicted. Since the author indicates that it is more likely only the ultimate stress will be known, these results are favorable. Since these results were similar for both test specimens this might be a model that could show acceptable results.

For the construction of the model when only the ultimate stress is known, the value for k used was 3.0, based on a best-fit analysis of the strain versus stress analysis, with an average coefficient of correlation of about 99%. Values of k were reported by the author to be 2.2 and 2.7; thus the average value would be about 2.45, but from the understanding of the paper, k values were determined for each specimen and averaged.

Figure 4.4: Model prediction and test one when f_o & ε_o and when only f_o are known

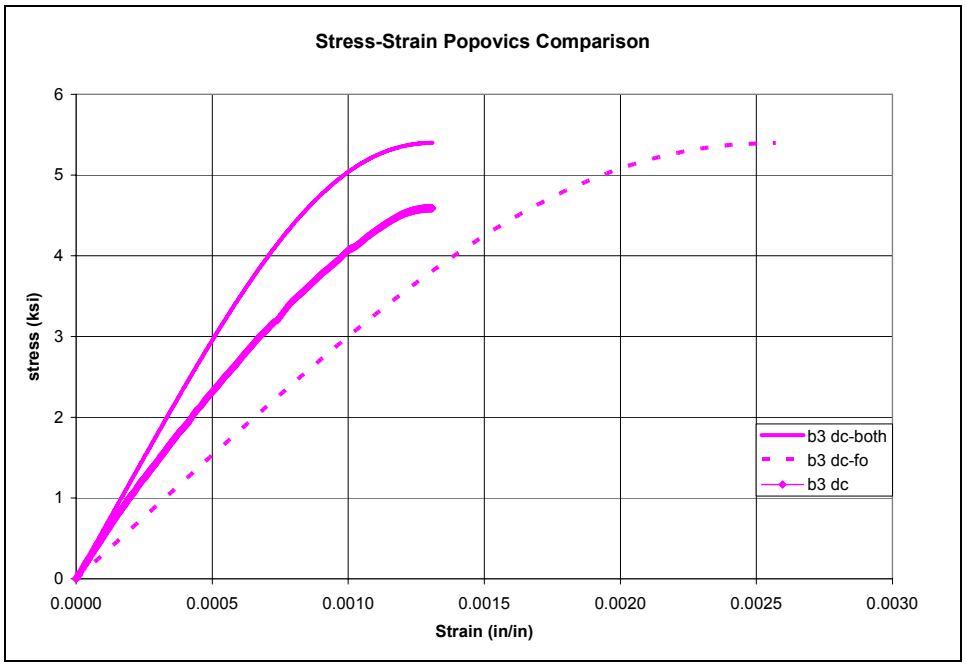

Figure 4.5: Model prediction and test two when f_o & ε_o and when only f_o are known

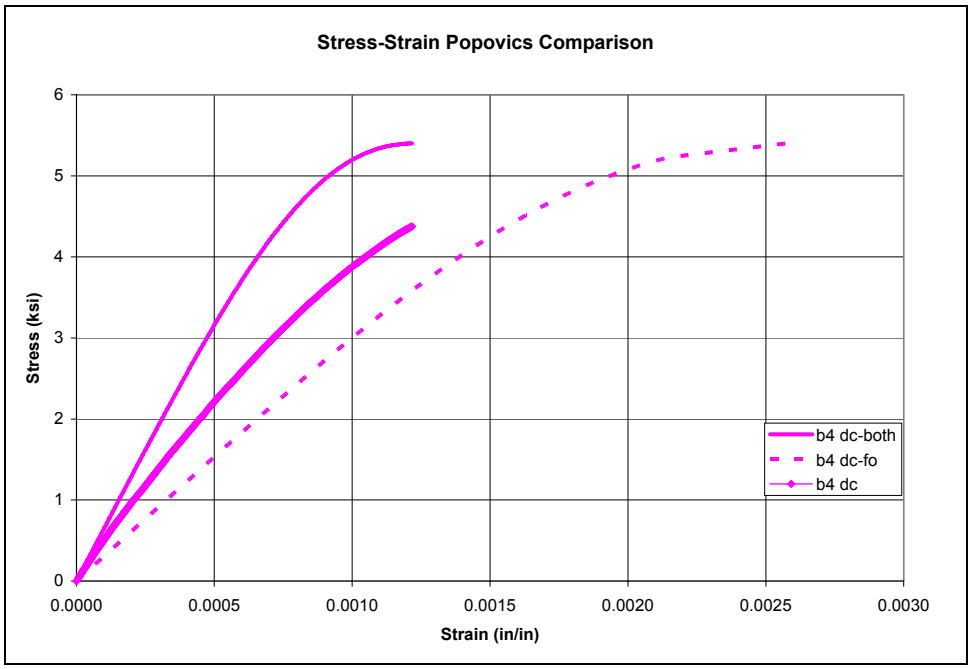

Mansur et al

Next, the model proposed by Mansur et al, which adjusts the global strain to local strain over plain, unconfined concrete, will be compared with the experimental results for plain, confined concrete. The comparison of the experimental data for the force-controlled specimens and the model's prediction of the actual stress-strain diagrams based on the data received from the potentiometers is shown below. From Figure 4.6 it can be seen that the stress-strain diagram as predicted does not completely match up with stress-strain diagrams as measured at mid-height from the actual specimens when the specimens are measure in force control mode with constant stress. Figure 4.7 shows the stress-strain diagrams which were constructed from the strain that was measured from the central portion of the displacement controlled specimens and compares these results with the predictions for the local stress-strain diagrams from the model. There is variance in both graphs between the model's predictions and the experimental test data.

Figure 4.6: Predicted diagrams of force controlled specimens and test diagrams

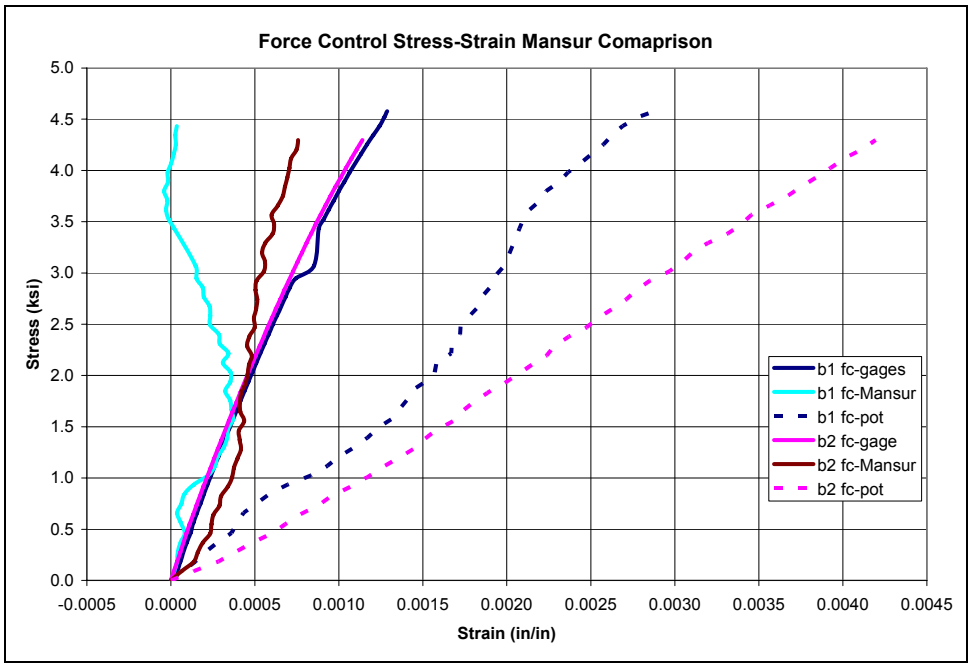

Figure 4.7: Displacement controlled specimens compared with model predictions

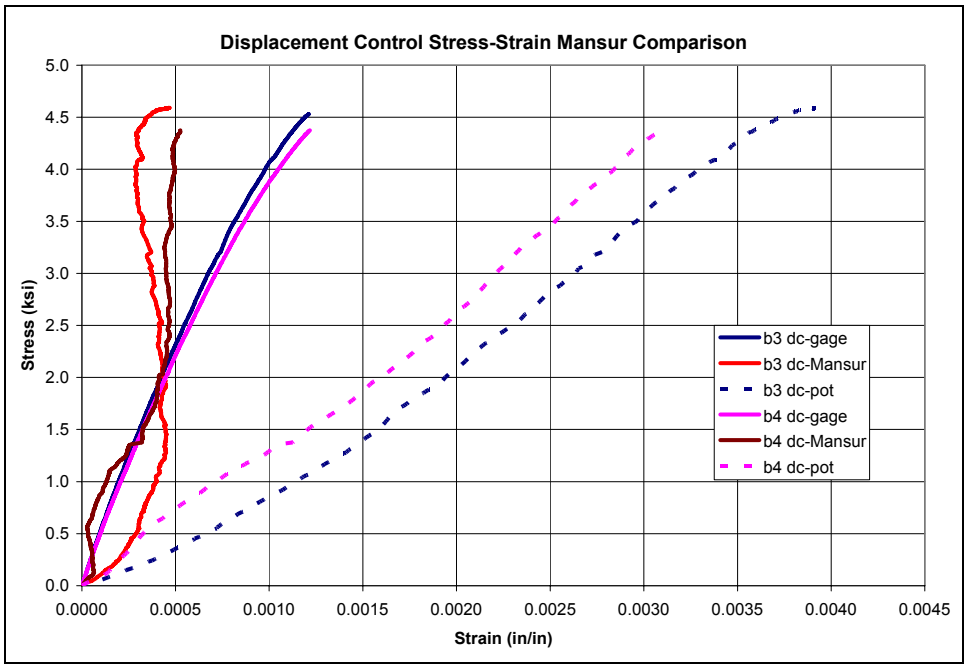

Toutanji

In the model proposed by Toutanji, a bilinear relationship for stresses and strains is determined for FRP-confined specimens. Figure 4.8 shows the prediction of the stress-strain diagram compared with the experimental data. The correlation appears to be within

acceptable tolerance. The model is conservative in the predictions, at least as compared with the four specimens that were not loaded to failure. This model does not attempt to predict the ultimate stress and strain, thus the comparison above does not have a specific end point. So the second branch of the comparison could, in theory, continue up to the ultimate rupture strain of the confinement; this would result in an ultimate confined stress of about 12 ksi.

Figure 4.8: Model's predicted stress-strain diagram compared with the test data

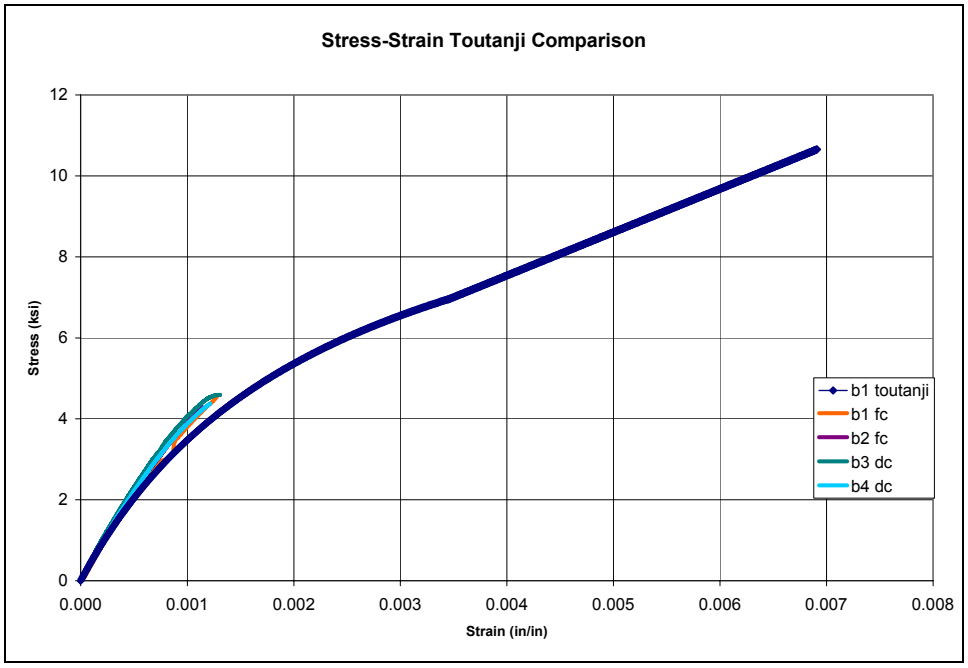

To construct this model, the confinement properties were required, as provided by the manufacturer. This allowed for the calculation of the lateral confining pressure, which was used to calculate the axial stress along the second branch. Once this was known, the axial strain corresponding to the axial stress along the second branch was determined. Using the confining pressure, the transition stress and strain were calculated followed by the stress for the first branch. All the equations provided by the author were determined with the intent that MPa would be used as the unit of pressure. Once all the stresses and strains were determined with the metric unit of pressure, a conversion factor to get the units in ksi was applied to the stress; this allowed the experimental data to be compared with the model's predicted stress-strain diagram.

Berthet et al

This model constructs a bilinear relationship for FRP-confined concrete, predicting the ultimate stress and strain, then the second branch of the stress-strain diagram followed by the first branch. The ultimate strain is predicted as a function of the lateral confining pressure, ultimate stress and strain of unconfined concrete, ultimate FRP strain and the relationship between radial and axial strain as in Equation 35. The ultimate confined stress is predicted with the ultimate unconfined stress and a variation of the equation proposed by Richert et al as a function of the lateral confining pressure and ultimate FRP strain, as can be seen in Equation 32. The stress for the second branch has been determined using Equation 41, when the strain is greater than ε_{ap}, the transition strain. Then Equation 49 was used to construct the first branch of the stress-strain diagram of the proposed model up to the transition strain. This equation is similar to that proposed by Toutanji with different boundary conditions and coefficients.

This model has a bit of a glitch. The equations used to determine the ultimate stress and strain and those that are used to calculate the second branch of the stress-strain diagram show a discrepancy. Figure 4.9 shows the complete stress-strain diagram as predicted by the model and the results of the experimental data collected from the first round of tests. This model was constructed to calculate the ultimate stress and strain with the appropriate equations, Equation 32 and Equation 35, respectively. Then, the second branch of the stress-strain diagram was constructed using Equation 41, to calculate every value of stress along the second branch the stress up to the ultimate strain. It is here where the problem arises. Since the ultimate stress and ultimate strain are predicted, the second branch of the stress-strain diagram should end at the ultimate stress and ultimate strain prediction, but it does not.

The formulation of the second branch has been evaluated and the error in determining the shape of the second branch must be in the calculation of θ_r, since it is this variable that controls the shape of the stress-strain diagram. This variable is a function of the confinement modulus which was determined based on a regression analysis of experimental data conducted by the authors for the two different types of carbon FRPs and E-glass FRP with a 99% coefficient of determination.

Figure 4.9: Model's predicted stress-strain diagram and test data for all specimens

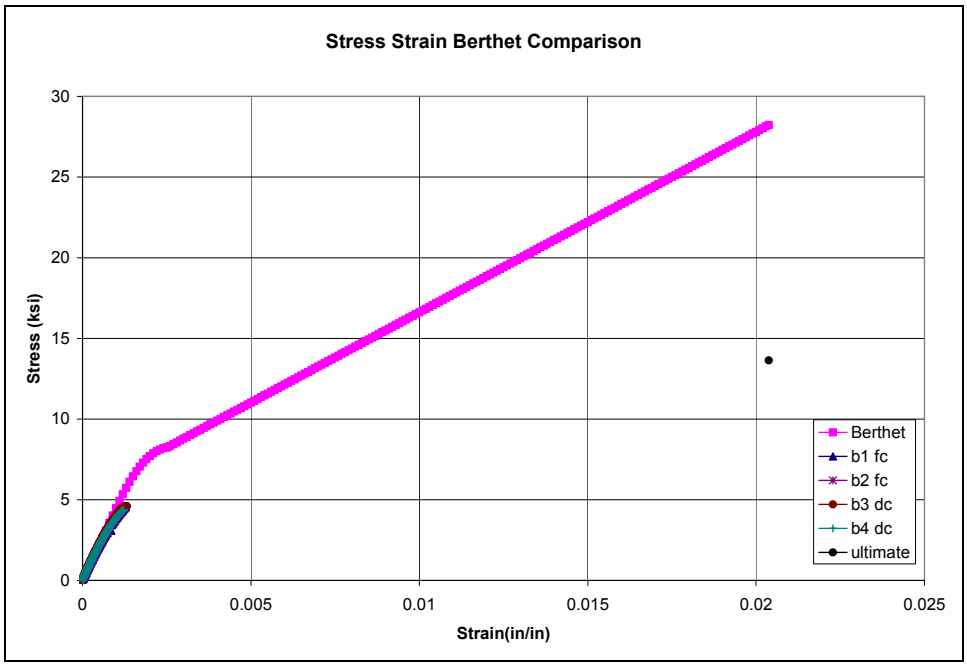

Attempts were made to contact the authors, to help clear up the discrepancy of the second branch at the ultimate stress and ultimate strain values. However, as of this writing, they have not responded for the clarification of the model.

Teng & Lam

In the design-oriented model proposed by Lam and Teng in 2003, the effect due to the stiffness of the FRP jacket is added as a parameter that controls the initial shape of the stress-strain diagram. The stress is determined based on two equations using the idea of Richard and Abbot's four parameter method. The actual confining pressure, based on test data from open literature and experimental testing conducted by the authors, was determined as a function of the ultimate FRP strain and modulus as provided by the manufacturer as well as the thickness of the FRP and the diameter of the concrete core. The ultimate confined stress is determined and it should be noted again that if substantial strength improvement is desired, the minimum actual confinement ratio $f_{l,a}/f'_{co}$ should be at least 0.07, otherwise the strength increase is of no consequence. Then the ultimate confined strain is determined. Then the modulus for the linear second branch of the stress-strain diagram is determined, allowing for the transition strain to be calculated.

Figure 4.10 shows the comparison of the predicted stress-strain curve by Lam and Teng (represented by the line with data points) with the actual test data.

Figure 4.10: Comparison of Lam & Teng prediction with experimental data

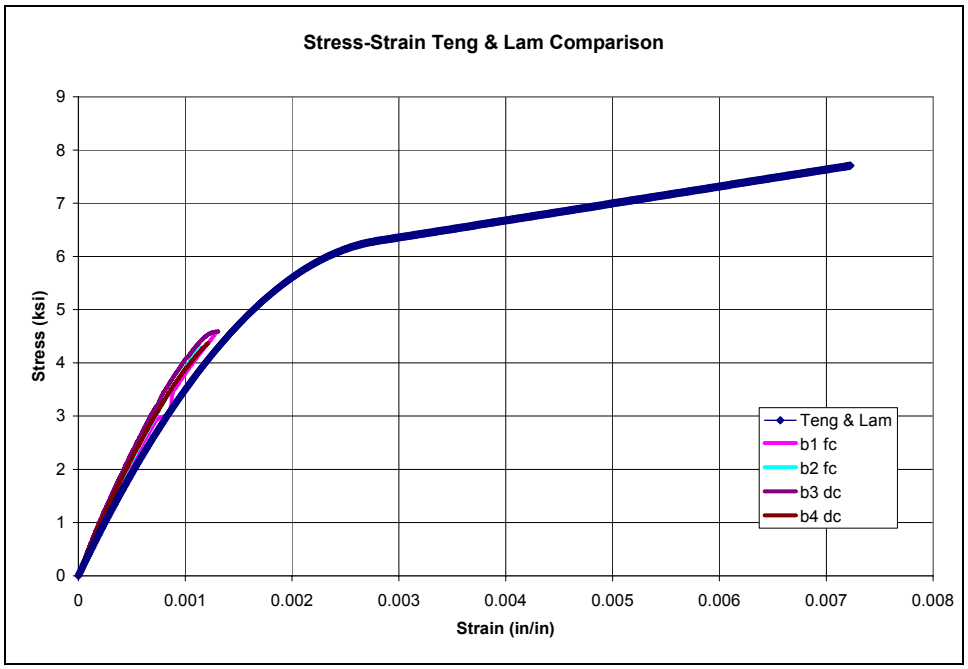

There is good correlation with the model and the test data. The model conservatively predicts the stress-strain relationship up to the point where the tests had to be prematurely terminated.

If at first we don't succeed we try, try again!—Round Two

Here, the test data from the second round of testing will be compared with the five models proposed by Popovics, Mansur et al, Toutanji, Berthet et al and Teng and Lam. The displacement rate for this round of tests was set at a constant strain rate equaling 0.0167 inches/minute throughout the testing and data collection process. All the strain data was recorded along with the load and displacement—through two methods of measuring. This information was used to construct the stress-strain curve and compare it with the models. Conclusions about the models' validity will be made in the next chapter.

Popovics

Since the tests were only conducted with a constant strain rate and the idea behind this model is that there was a difference in the shape of the stress-strain diagram if the

specimens were loaded at either a constant rate of stress or constant rate of strain, no comparisons can be made about the difference in shape. However, the experimental data can be compared with the model's predictions to determine if there is any accuracy or consistency in the model's prediction of the stress-strain diagram for the second round of testing. Figure 4.11 shows the predicted stress-strain value based on the model with both the ultimate stress and ultimate strain known, and compares it with the experimental data. Reviewing Figure 4.11, it can be seen from the data that the model does not predict the actual stress-strain relationship well.

Figure 4.11: Compares the model's predictions with the experimental test data

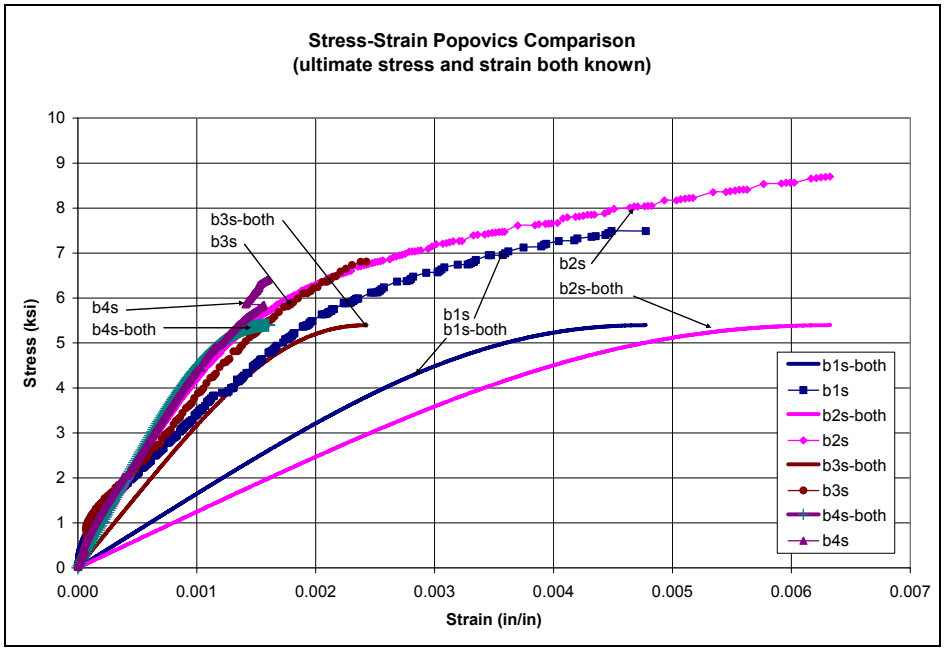

It can also be seen, from Figure 4.12, that the stress-strain relationship predicted by the model results in the exact same correlation no matter which specimen is being represented. This is because the model does not use any of the strain information from the specimens, and since the ultimate strain is a function of the unconfined ultimate stress and the *k* value, which is the same for all four specimens, it would seem reasonable that the relationship for all of these would result in identical curves.

Figure 4.12: Comparison of model predictions with test data when only f_o is known

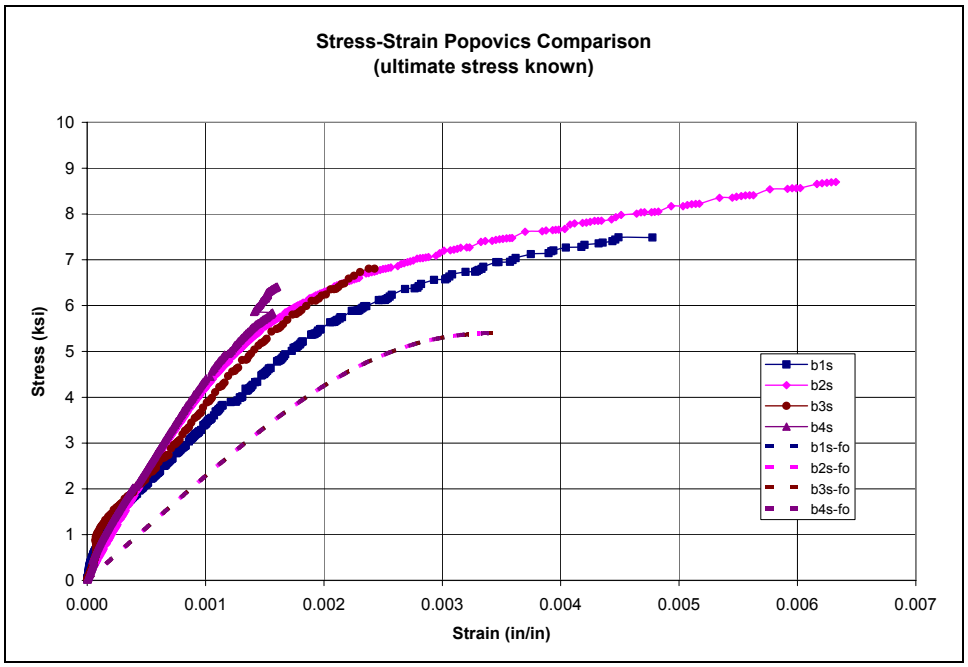

Mansur et al

The model proposed will attempt to adjust the deformation due, not only to the specimen, but also to deformation resulting from the testing machine. This is completed by measuring the deformation over the entire length of the specimen and converting it to strain, in addition to measuring the strain at the central portion of the specimen. For this model to work, the authors note that the strain must also be collected over the central portion of the specimen, because the initial modulus is a required part of the formula. Figure 4.13 shows the comparison between the stress and strain as predicted by the model, with that of the actual stress and strain of the experimental data as measured from the central portion of the specimen. While in three of the four specimens the strain is predicted to be greater than the actual strain, in two of the three, it is only slightly larger, and is dramatically greater in the last specimen. In these cases, the model is conservative in its prediction of the strain at a given stress, and the general trend of the model is one of conservativeness. With the exception of specimen b3s, the actual stress-strain relationship results in a higher stress than that predicted for a given strain, allowing for "conservative" to be used as the description of the model.

Figure 4.13: Comparing model predictions with test data

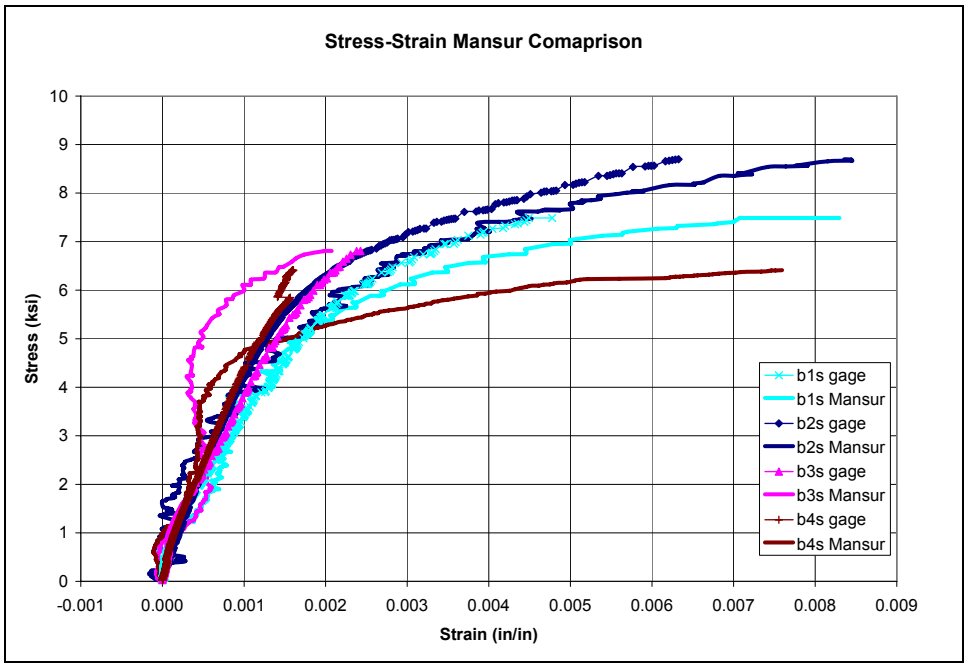

This model is based on knowing the strain at the central portion of the specimens, at least for the beginning of the testing, but the majority of the data known must come from the potentiometers or transducers measuring the global displacement and converting the measurements to strain over the entire length of the specimens. As can be seen in the above figure, the predicted stress-strain diagram is not a smooth curve. This is due to the potentiometers, the data acquisition system, the way in which the data acquisition system collected the data, and the way the potentiometers measured the data. Attempts to smooth the curve resulted in numerous data points being lost and it was decided that to ensure the authenticity of the data, the unadjusted or rather little adjusted stress-strain curve be shown instead of the stress-strain diagram that would be similar to that seen in Figure 4.14. This figure shows the original prediction with a solid line, and the adjusted prediction with the solid line with data points; the actual stress-strain relationship as measured from the central portion of the specimen is represented by the dashed line and the dotted line shows the strain as measured globally from the potentiometers for one specimen. It can be seen that a significant number of data points are lost from stresses of about 2 ksi to 5.5 ksi and the shape does not improve much.

Figure 4.14: Adjusted stress-strain prediction compared with test data

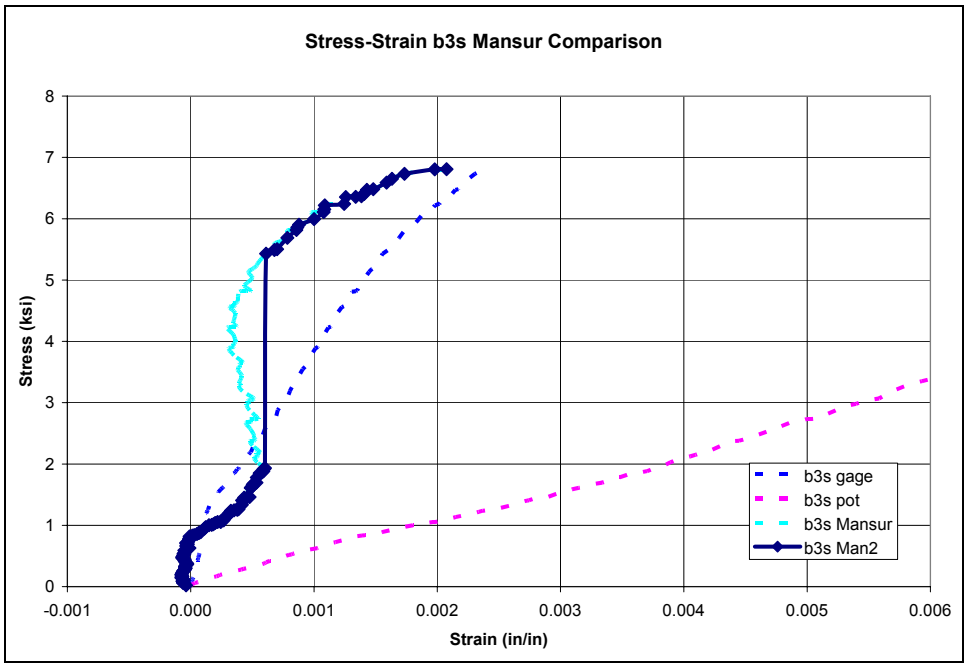

The relative shape of the predicted stress-strain diagram for specimens labeled "b1s" and "b2s" is closely related to that of the actual experimental data, and can be seen in Figure 4.15, while the shape of the stress-strain diagram for specimens marked "b3s" and "b4s" do not particularly match the experimental data as is depicted in Figure 4.16.

Figure 4.15: Predictions and test data for specimens named b1s and b2s

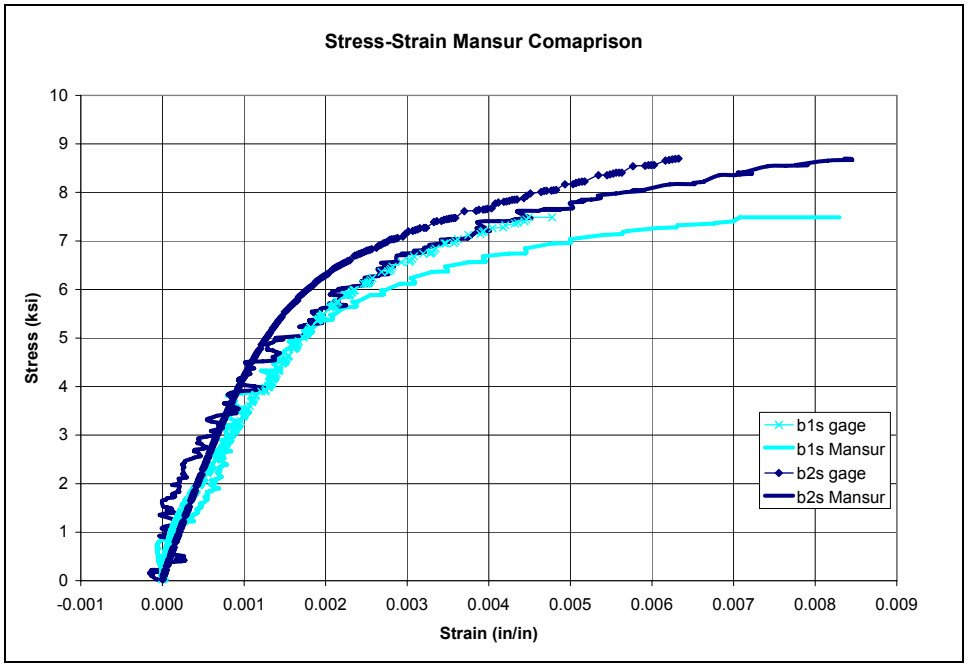

Figure 4.16: Predicted stress-strain curves and test data for specimens b3s and b4s

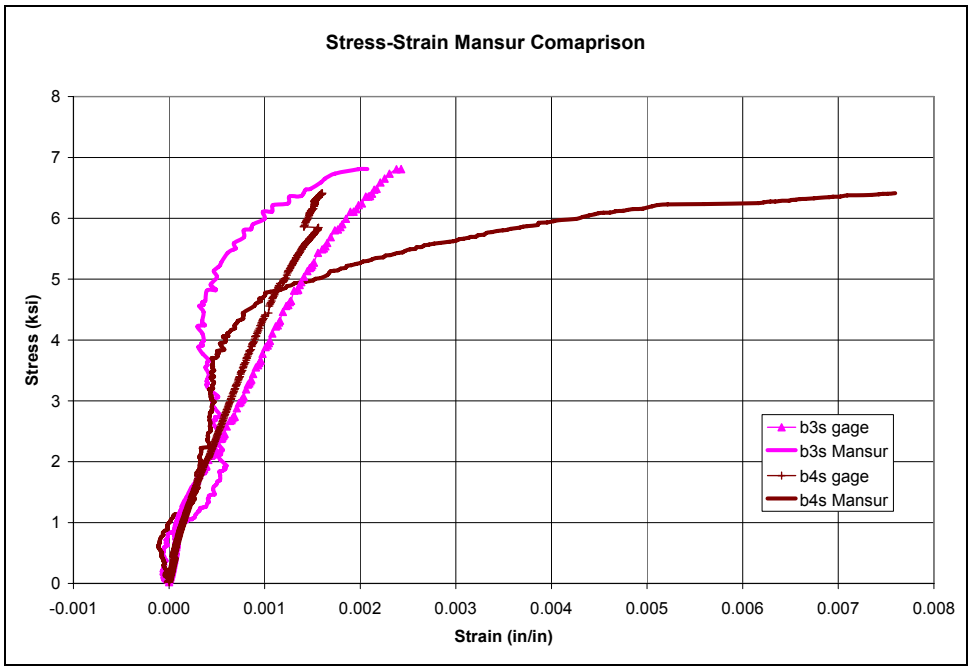

Since there was no difference in the testing of the specimens during the second round of tests and they were all loaded in displacement control with the same loading rate, the only explanation for this variance is load history. Specimens named "b3" and "b4" were loaded in displacement control during the first round of tests, while specimens labeled b1 and b2 were loaded in force control. It would appear that this slight difference plays a noteworthy role in how accurately the model predicts the stress-strain relationship.

Toutanji

The relationship of stress-to-strain for confined concrete as predicted by this model is illustrated in Figure 4.17 and compared with the experimental data. Since this model does not predict the ultimate stress and ultimate strain, the values which were used to create the model were arbitrarily ended.

Figure 4.17: Compares data from specimens with model's prediction

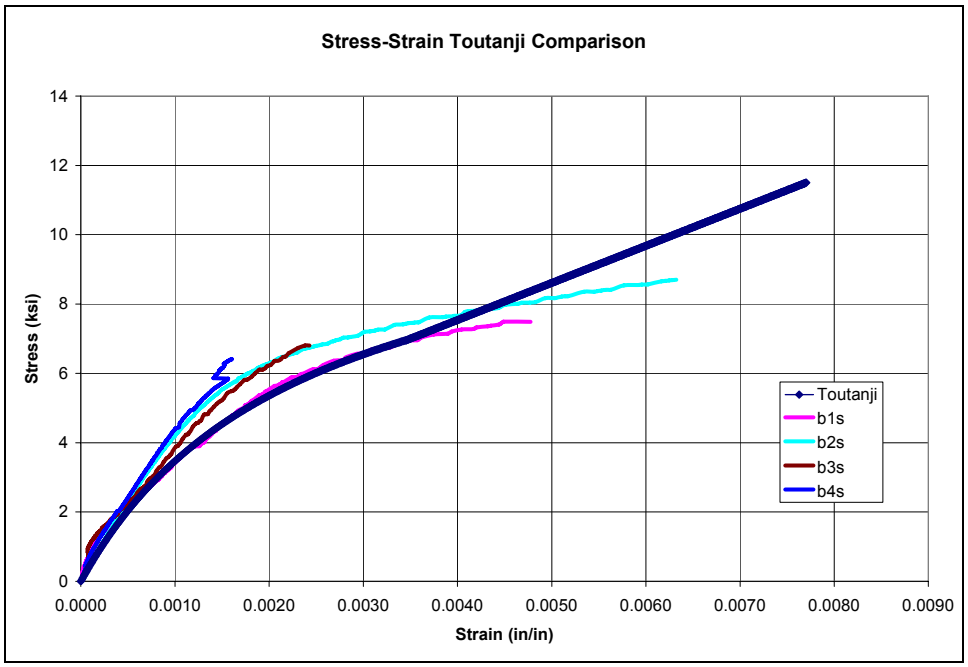

This model shows relatively good correlations with the experimental data. It is also on the conservative side, for the most part. Since specimens identified as "b1s" and "b2s" have strains that are greater than that predicted by the model at given stresses near the end of the testing, this shows that the model is not completely conservative or does not take enough parameters into consideration. Specimens labeled "b3s" and "b4s" show that throughout the experiment, the model is completely conservative. A possible reason, for the specimens that showed strains greater than that predicted by the model, could be the load history. These specimens were previously loaded in force control, then loaded to failure in displacement control, while the specimens that show that the model is conservative were loaded throughout both tests in displacement control.

This model was created based on test data that were generated in force control with a constant load rate of about 13.5 kips/minute, so it is noted that the model is not conservative toward the end of the tests, when compared with the experimental data that was originally loaded in force control mode.

Berthet et al

As was noted above, this model has a bit of a problem. The ultimate stress and ultimate strain as predicted by the model and the end of the second branch at the "so-

called" ultimate strain do not reflect the ultimate stress at this "so-called" ultimate strain. Figure 4.18 shows the discrepancy in the model, as well as how the model compares with the experimental data. From inspection of the model prediction it appears that there is a problem with the shape and smoothness of the transition between the first and second branch. From initially inspecting Figure 4.18, it would appear that if there were a line connecting the transition point to the ultimate point, the second branch of the stress-strain diagram would seamlessly join the first and second branches. This would make the second branch nearly tangent to the end of the first branch, as can be seen in Figure 4.19.

Figure 4.18: Prediction of stress-strain relationship compared with test data

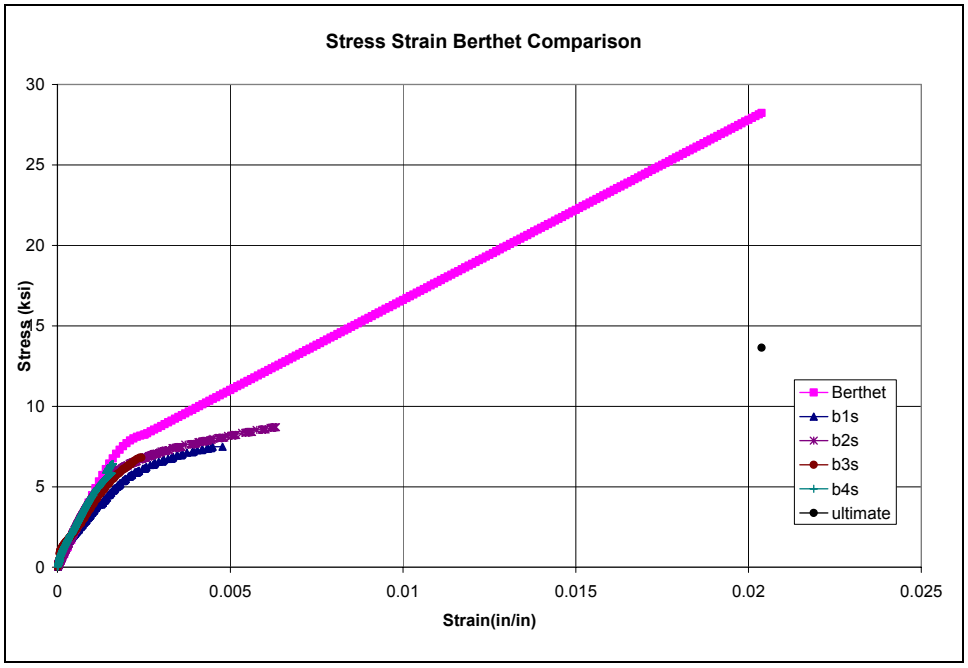

Figure 4.19: Model predictions compared with test data and adjusted second branch

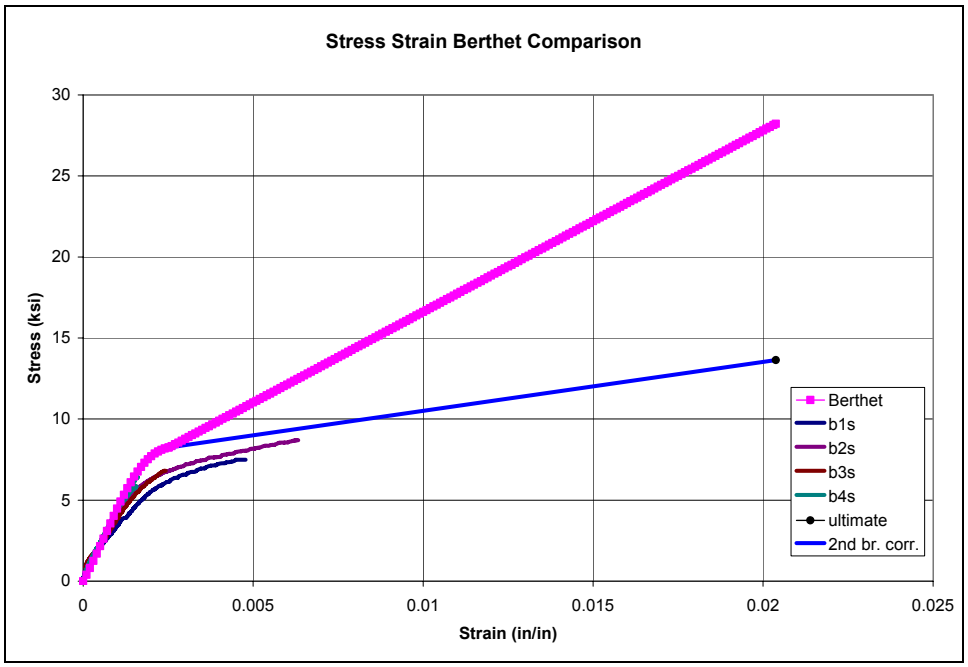

The problem with this model is the equation for determining the stress at a strain greater than the transition strain for the second branch. Since this equation is multi-functional, it has been deduced that the likely culprits causing the error in the formulation of the second branch would be the calculation of the slope of the line, θ_r or γ, the ratio of plastic strain. The latter of these two parameters was picked because of an issue with the units. This is a ratio and thus should be unitless; however, the confinement modulus is in units of MPa and the unconfined compressive stress is in units of MPa, which will be squared all to the negative two-thirds power.

Teng & Lam

The comparison of the stress-strain diagram, as predicted by the model proposed and the experimental test data, is displayed below in Figure 4.20. There is good correlation with the test data throughout the entire data set for each of the specimens. The specimens that were previously loaded in force control during the first round of testing show the linear second branch of the test well, and have relatively similar slopes compared to that of the predicted slope of the second branch.

Figure 4.20: 2nd round model prediction compared with test data

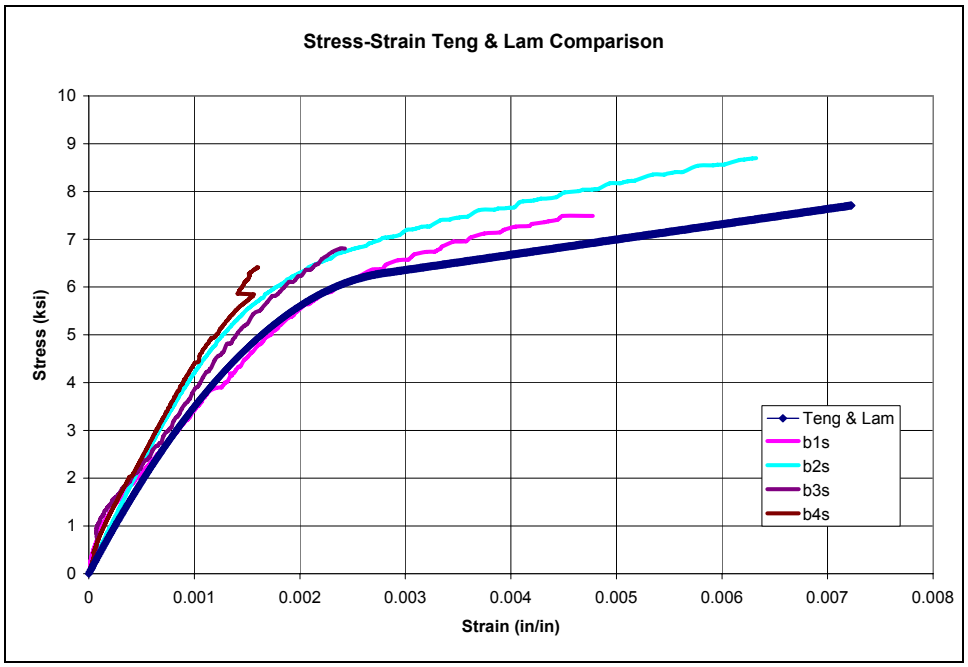

CHAPTER 5 - Conclusion

Four concrete specimens, with an average unconfined compressive strength about 5.4 ksi at the time of testing, were used to construct confined specimens. These specimens had three longitudinal strain gauges applied to the surface of the concrete at mid-height about 120° apart, in addition to two radial strain gauges also applied at mid-height about 180° apart. All the specimens were wrapped with two continuous layers of carbon fiber which had been impregnated with a two-part epoxy resin-hardener system. The epoxy was allowed to cure for one day before the testing began.

Due to the fact that the testing apparatus was not capable of producing a load that would allow for the failure of the FRP-confined concrete, because the core concrete had a higher strength than was ordered from the concrete company, two rounds of testing were conducted. During the first round of tests, two of the specimens were tested with a constant load rate, equivalent to 60 kips/minute; while two others were conducted at a rate of 0.0067 inches/minute, keeping a constant deformation rate. Once the testing had taken place, the data was used to determine if the existing models—to which this paper has made reference for comparison—are valid, need improvement or recommendations

or are completely defective or inconsistent. Initial conclusions from the first round of testing were made to be:

As noted by Popovics (1973), the adjustment for the stress-strain diagram only is understandable for data which was collected with a constant strain rate. Comparing the strain measurements for the specimens when the test was conducted under a load-control or a displacement-control protocol resulted in no noticeable difference in the shape of the stress-strain diagram. Comparison with the experimental data with the specimens that were loaded at a constant strain rate, as the author indicates for which the model is supposed to be valid, results in one of two outcomes, depending on which method was used to construct the model. The first is that if both the ultimate stress and ultimate strain are known, the model is not conservative. Only if the ultimate stress is known is the model is conservative. This works well, because the author notes that in most cases only the ultimate stress is known, regardless of how the strain was collected—locally at the central portion or globally over the entire length of the specimens.

The model proposed by Mansur et al (1994) does not fit the experimental data well for adjusting the global strain to local strain. It does not appear to matter whether the specimens were loaded with a constant strain rate or a constant stress rate. There appears to be no correlation between the strain as measured by the gauges at the central portion of the specimens and the strain as predicted by the model to represent the actual strain of the specimen. This model was intended to be used with plain, unconfined concrete. So, it may be possible that the model, considering its intended use, cannot be extrapolated to other uses, like confined concrete.

The model proposed by Toutanji (1999) is conservative and the experimental data correlates well with the model. The model, however, does not predict the ultimate values for stress and strain. These parameters should be included in the model and would add to the integrity and applicability of the model. At its existing conditions, there is no way to know the type of failure for the specimens, since the ultimate values are not predicted by the model.

The model proposed by Berthet et al (2005, 2006) appears to match for most of the first branch of the stress-strain diagram; however, it seems to over-predict the stress and strain at the transition point, meaning that the stress predicted by the model at a given

strain is greater than the stress of the test specimens. It is also clear that the ultimate stress and ultimate strain deviate largely from the actual experimental data. Even though this data does not include the failure point, it is clear that the ultimate stress and strain value is going to be too high. It is also apparent that this model has some discontinuity between the end of the second branch and that of the ultimate stress and strain point. This discontinuity could be a result of two parameters which were used to construct the second branch of the stress-strain diagram. Attempts at contacting the authors have been made to try to resolve this problem, with no success as of yet. It also seems that the model is not sensitive to the method of strain measurement; namely if the strain is calculated from the strain measured from the potentiometers or for the central region of the specimens with the strain gauges.

In the model proposed by Lam and Teng (2003, 2004) there is good agreement throughout the initial round of testing. The beginning portion the stress-strain prediction and the actual experimental data correlate very well, and when divergence begins, the model provides conservative predictions.

For the second round of testing, the four specimens were fitted in the newly constructed nutcracker-like device. This device ensured that there would be enough force to load the specimens to failure. The loading rate, in a displacement control loading regime, was increased to 0.0167 inches/minute. Once the remaining data had been collected and analyzed, comparisons with the new data were made in relation to the aforementioned models for the stress-strain relationships of confined concrete. The conclusions about each of the models' performance in comparison with the experimental data are as follows:

The model proposed by Popovics (1973) is only valid for tests conducted in displacement control or at a constant strain. However, the specimens were all compared with the predictions based on both ultimate stress and ultimate strain known and with only the ultimate stress known. With the data set from the second round of testing, it appears that when both the ultimate stress and ultimate strain are known, there is a difference in whether the specimens were previously loaded with a constant stress rate or a constant strain rate. For the specimens that were loaded with a constant stress, the model is very conservative. It would be so conservative that the results from the model

would likely not even be useful, because the initial modulus does not even come close to matching the model's predictions, which is usually the case. It is agreed upon that the behavior of confined concrete is nearly identical to that of unconfined concrete up to the point where the FRP becomes engaged; since this is not the case for the specimens that were previously loaded with a constant rate of stress, it would be appropriate to say that this model does not fit when the specimens have been previously loaded with a constant rate of stress, and that load history plays a key role in the shape of the stress-strain diagram. The predictions for the specimens that were loaded both times with a constant strain are conservative, but such that they would probably provide relatively accurate results. It can be seen with specimen b4s that the prediction is almost identical to the actual data. This could be in part due to the fact that this specimen failed at a relatively low stress when compared to the other specimens.

For specimens when only the ultimate stress is known, the shape of the stress-strain diagram will be exactly the same for specimens with the same k value. The initial modulus is not predicted well with respect to the experimental data. This raises some cause for concern about the validity of this model for confined concrete; however, the model shows conservativeness. Even though the model proposed by Popovics (1973) is not intended to be used for confined concrete, it is possible for the model to generally predict the stress-strain diagram up to the ultimate unconfined compressive stress on the conservative side. However, one would be wise to use the predicted stress-strain diagram from this model as a starting point, and incorporate a model that is more suitable for predicting the stress-strain relationship of confined concrete.

The model proposed by Mansur et al (1994) shows some promise for getting a rough estimate of the actual strain as would be measured at the central portion of the specimens when the predominate form of measurement of strain is globally. This approach of measurement is used, because the actual strain at the central portion of the specimen is needed for calculating the initial modulus of elasticity. The smoothness of the model, or lack thereof, is likely due to the data acquisition system and the potentiometers. The attempt to smooth the curve resulted in a significant loss of data in the initial portions of the stress-strain diagram. It is evident from the data and the model predictions that the level accuracy with which the model will predict the stress-strain

relationship is affected by the load history. For the specimens that were loaded with a constant rate of strain during both rounds of testing, the model's predictions are sporadic and irregular in shape, independent of the lack of smoothness, while the specimens that were first loaded with a constant rate of stress and then loaded with a constant rate of strain show a close general correlation to the actual data. However, the results from the first round of testing showed that there was no correlation at all. This may lead one to the conclusion that other parameters should be included in the formulation of the model, such as load history.

The model proposed by Toutanji (1999) was constructed by first calculating the second branch of the stress-strain diagram, followed by the first branch and then the transition points. These two sections were combined to form one continuous stress-strain diagram with a smooth transition. The relative shape of the stress-strain diagram of the experimental test data is similar to that of the model. The results from the model are conservative. It should be noted here, as well, that for the specimens that were first loaded with a constant stress, compared to those with a constant strain, the model does not accurately or conservatively predict the end of stress-strain diagram even though this model was created based on loading with a constant rate of stress. No ultimate points were determined by the model which allows one to draw the conclusion that the ultimate strain should be that of the FRP. In most cases this is provided by the manufacturer and has been reported by some as not realistic of the actual behavior.

The model proposed by Berthet et al (2005, 2006) has some problems. The ultimate stress and strain are predicted first, followed by the second branch for every point greater than the transition strain up to the ultimate strain. Finally, the first branch is predicted up to the transition strain. The first concern is with the fact that the ultimate stress and strain value do not match up with the ultimate stress, according to the formulation of the second branch at the ultimate strain value. Then, even if the second branch were tangential to the first branch and ended at the ultimate stress and ultimate strain point, the experimental data shows that the model is not conservative and over-predicts the stress in addition to grossly over-predicting the ultimate strain.

The model proposed by Lam and Teng (2003, 2004) is in great agreement with the experimental data. The stress and strain values are conservatively predicted when

compared with the test data throughout. It does appear that load history plays a part in the shape of the stress-strain diagram, which has not yet been addressed by this model.

So, in general, some models are more accurate in predicting the stress-strain response of confined concrete when compared with the test specimens in this study. However, this does not certify the general accuracy and applicability of one model against others. Most of the models developed by various researchers are based on their experimental data which has been conducted under some controlled laboratory environments. This controlled environment definitely affects the experimental results and may not be accurately reflected in the models. So, these models will fail in predicting the stress-strain performance of specimens tested under a different laboratory conditions. However, there are some models that have been developed, addressing the aforesaid fact; these models are expected to be more versatile. While a few of these models may give reasonable accuracy in their predictions, most of them need to implement more real-world parameters, such as the effect of sustained loading and the arrangement of longitudinal and transverse reinforcement in the specimens, in their models for a better accuracy and more realistic prediction.

References

Berthet, J.F.; Ferrier, E. and Hamelin, P.; "Compressive behavior of concrete externally confined by composite jackets Part A: Experimental study" *Construction and Building Materials*, v 19, n 3, April, 2005, p 223-232

Berthet, JF; Ferrier, and E.; Hamelin, P.; "Compressive behavior of concrete externally confined by composite jackets Part B: Modeling" *Construction and Building Materials*, v 20, n 5, June 2006, p 338-347

Berthet, JF et al; "Modeling of the creep behavior of FRP confined short concrete columns under compressive loading" *Materials and Structures*, v 39, 2006, p 53-62

Lam, L.; Teng, J.G.; "Design-oriented stress-strain model for FRP confined concrete" *Construction and Building Materials*, v17, n 6-7, September-October 2003, p 471-489

Loov, Robert, E.; "Reinforced Concrete at the Turn of the Century" *Concrete International*, December 1991, p 67-73

Lorenzis, L.; "A comparative study of models on confinement of concrete cylinders with FRP composites" Division of Building Technology Chalmers University of Technology, work no 46, publication 01:04, 2001, p 1-73

Lorenzis, L.; "A comparative study of models on confinement of concrete cylinders with FRP composites" *Journal of Composites for Construction*, v 7, n 3, August, 2003, p 219-237

Mansur, M.A., Wee, T.H. and Chin, M.S.; "Derivation of the Compete Stress-Strain Curves for Concrete in Compression", *Magazine of Concrete Research*, v 47, n 173, Dec 1995, p 285-290

Mansur, M.A., Chin, M.S., Wee, T.H.; "Stress-Strain Relationship of High-Strength Fiber Concrete in Compression", *Journal of Materials in Civil Engineering*, v 11, n 1 Feb 1999, p 21-29

Matthys, S.; Toutanji, H.; Taerwe, L.; "Stress-strain behavior of large scale circular columns confined with FRP composites" *Journal of Structural Engineering*, v 132, n 1, January 2006

Nawy, Edward G.; *Reinforced Concrete: A Fundamental Approach*. 5th ed. New Jersey: Pearson Education, Inc, 2005.

Popovics, S,; "Review of Stress-Strain Relationships for Concrete" *Journal of the American Concrete Institute*, v 67, n 3, 1970, p 243-248

Popovics, S.; "A numerical approach to the complete stress-strain curve of concrete" *Cement and Concrete Research*, v 3, 1973, p 583-599

Sakai, Junichi; "Unloading and Reloading Stress-Strain Model for Confined Concrete", *Journal of Structural Engineering*, v 132, n 1, 2006, p 112-122

Teng, J.G.; Lam, L.; "Behavior and Modeling of Fiber Reinforced Polymer-Confined Concrete" *Journal of Structural Engineering*, v 130, n 11, November 2004, p 1713-1723

Toutanji, Houssam A.; "Stress-strain characteristics of concrete columns externally confined with advanced fiber composite sheets" *ACI Materials Journal*, v 96, n 3, May-June 1999, p 397-404

Appendix A - Notations

f = axial stress

E = initial modulus of elasticity

ε = strain

ε_o = strain at ultimate stress (f_o)

f_o = ultimate stress

n = function of compressive strength of normal weight concrete given by

$$n_{concrete} = 0.4x10^{-3} f_o + 1.0$$

k = function of the type of mineral aggregate used and the applied test method ($in^{1/2}/lb^{1/4}$)

E_l = lateral elastic modulus

ε_l = lateral strain of the confined specimens

E_{frp} = elastic modulus of the FRP as provided by the manufacturer

t = thickness of the FRP

R = radius of the cylinder

f_{cc} = confined concrete strength

f'_c = ultimate unconfined concrete stress

k_1 = confinement effectiveness coefficient

f'_l = lateral pressure

f_a = calculated axial stress

f_l = lateral stress applied to the concrete by the FRP

ε_{ca} = axial strain in strength of confined concrete

ε_a = axial strain of specimens,

k_2 = concrete strain enhancement coefficient and can be calculated by

$$k_2 = 310.57\varepsilon_l + 1.90$$

E_{ia} = initial tangent of modulus of elasticity of $f_a - \varepsilon_a$ curve

f_{ua} = axial stress between elastic and plastic regions

ε_{ua} = strain between the elastic and plastic regions in the axial direction

E_{ua} = tangent of modulus of elasticity between elastic and plastic regions of $f_a - \varepsilon_a$ curve

f'_{cc} = ultimate confined concrete strength

f'_{co} = ultimate unconfined compressive concrete strength

k_1 = efficiency ratio

f_{lu} = ultimate confinement pressure

f_l = lateral confining stress

E_{frp} = modulus of elasticity of the FRP as provided by the manufacturer

ε_r = radial strain

t = thickness of the FRP

r = radius of the concrete core

f_{lu} = ultimate lateral confining stress

ε_{fu} = ultimate radial strain as provided by the manufacturer

E_l = confinement modulus of elasticity

Δf_l = change in confining stress

$\Delta \varepsilon_r$ = change in radial strain

E_{frp} = Young's modulus of confinement of the FRP

γ = plastic strain ratio

f'_{co} = unconfined compressive strength of concrete

ε_{au} = ultimate axial strain of confined concrete

ε_{ao} = ultimate axial strain of unconfined concrete (typically taken to be 0.002 inch/inch)

ε_{fu} = ultimate FRP strain as provided by the manufacturer

v_c = Poison's ratio (typically taken to be 0.2)

θ_r = slope of the pseudo-plastic branch

f'_{cp} = reference plastic stress or the transition stress where the first and second branch intersect

ε_{rp} = radial strain at the intersection between the first and second branch (0.002 inch/inch)

ε_{ap} = axial plastic strain corresponding to ε_{rp}

ε_{ao} = unconfined compressive strain (typically 0.002 inch/inch)

ε_{ro} = radial strain of unconfined concrete

E^*_r = transverse equivalent modulus

E^*_a = equivalent elastic modulus

σ_h = hoop stress

E_{frp} = modulus of elasticity

ε_h = hoop strain of the FRP

$f_{l,a}$ = actual confining pressure

$\varepsilon_{h,rup}$ = hoop strain at rupture

f_o = reference stress

E_1 = initial modulus

E_2 = plastic modulus

n = shape parameter (control the transition between the first branch and second branch of the stress-strain diagram)

Appendix B - Popovics Computations

Table B.1 shows the typical calculations for the stress-strain diagram as predicted by Popovics when both the ultimate stress and ultimate strain of the specimen are known. The value *n* is calculated using Equation 2. The vale for f_o is from the experimental testing of the unconfined compressive strength. The value for the ultimate gage strain (ε) was determined from the experimental tests. The strain values were calculatingly entered and the stress was calculated using Equation 4.

Table B.1: Typical computations both ultimate stress and strain known

b1 fc - known ult. Stress & strain	
$n_{concrete}$=	3.1592
f_o (psi)=	5398
ult gage ε=	0.001241534

strain	stress
0.000000	0.000000
0.000025	0.159037
0.000050	0.318068
0.000075	0.477080
0.000100	0.636045
0.000125	0.794925
0.000150	0.953666
0.000175	1.112204
0.000200	1.270457
0.000225	1.428334
0.000250	1.585725
0.000275	1.742509
0.000300	1.898550
0.000325	2.053699
0.000350	2.207793
0.000375	2.360657
0.000400	2.512104
0.000425	2.661936
0.000450	2.809945
0.000475	2.955912
0.000500	3.099615
0.000525	3.240820
0.000550	3.379293
0.000575	3.514794
0.000600	3.647084

Cont.

strain	stress
0.000650	3.901074
0.000675	4.022305
0.000700	4.139390
0.000725	4.252113
0.000750	4.360266
0.000775	4.463656
0.000800	4.562103
0.000825	4.655442
0.000850	4.743527
0.000875	4.826229
0.000900	4.903440
0.000925	4.975072
0.000950	5.041060
0.000975	5.101359
0.001000	5.155945
0.001025	5.204820
0.001050	5.248003
0.001075	5.285537
0.001100	5.317486
0.001125	5.343932
0.001150	5.364976
0.001175	5.380736
0.001200	5.391347
0.001225	5.396958

Table B.2 shows typical calculations for the construction of the stress-strain diagram when only the ultimate stress is known, which is often the situation. The value for ε_o was determined using Equation 5, where the value for constant k was determined using a strain to stress correlation and a regression analysis equation. For first round, this value was determined to be 4 and for second round it was determined to be 3. Stress was again calculated using Equation 4. The data below only shows the stress calculation based on the value of k for the first round of testing and only shows a small portion of the data used to construct the stress-strain relationship for simplicity. Similar values are reported for the second round of testing.

Table B.2: Typical computations only ultimate stress known

b1 fc - only ult stress known	
$n_{concrete}$=	3.1592
f_o (psi)=	5398
ε_o=	0.0021429

strain	stress
0.000000	0.000000
0.000005	0.015357
0.000010	0.030714
0.000015	0.046071
0.000020	0.061428
0.000025	0.076785
0.000030	0.092142
0.000035	0.107499
0.000040	0.122856
0.000045	0.138213
0.000050	0.153570
0.000055	0.168927
0.000060	0.184284
0.000065	0.199641
0.000070	0.214997
0.000075	0.230354
0.000080	0.245711
0.000085	0.261067
0.000090	0.276424
0.000095	0.291780
0.000100	0.307136
0.000105	0.322492
0.000110	0.337848
0.000115	0.353203
0.000120	0.368558

Cont.

strain	stress
0.000125	0.383914
0.000130	0.399268
0.000135	0.414623
0.000140	0.429977
0.000145	0.445331
0.000150	0.460684
0.000155	0.476038
0.000160	0.491390
0.000165	0.506742
0.000170	0.522094
0.000175	0.537445
0.000180	0.552796
0.000185	0.568146
0.000190	0.583496
0.000195	0.598845
0.000200	0.614193
0.000205	0.629540
0.000210	0.644887
0.000215	0.660233
0.000220	0.675578
0.000225	0.690922
0.000230	0.706265
0.000235	0.721607

Data Continues…

Appendix C - Mansur et al Computations

Table C.1 shows the computations for one of the test specimens that were performed during the construction of the stress-strain diagram for this model. The moduli needed for this model, E_{co} and E_{dt}, were calculated based on the change in stress over the change in strain up to about $0.35f'_c$. The values for *pot strain* and *stress* were taken from the test data. Equation 9 was used to calculate the strain as predicted by the model, *Mansur corr strain*. This table shows the calculations as a representation of the other specimens and the second round of testing.

Table C.1: Typical model computations

b1 fc	
E_{co}	4251.837
E_{dt}	1199.5071

pot strain	stress	Mansur strain
0.000000	0.000000	0.000000
0.000075	0.091013	0.000020
0.000145	0.182498	0.000036
0.000209	0.280348	0.000042
0.000280	0.371833	0.000057
0.000361	0.463789	0.000083
0.000397	0.567299	0.000057
0.000432	0.658548	0.000038
0.000511	0.749325	0.000062
0.000585	0.842696	0.000081
0.000695	0.934180	0.000136
0.000835	1.025193	0.000221
0.000931	1.117385	0.000262
0.001002	1.207927	0.000279
0.001092	1.299412	0.000315
0.001168	1.390896	0.000336
0.001228	1.482381	0.000341
0.001312	1.573630	0.000370
0.001357	1.665114	0.000361
0.001405	1.757306	0.000353
0.001430	1.848555	0.000324
0.001515	1.939804	0.000354
0.001571	2.031289	0.000355
0.001580	2.123952	0.000309
0.001669	2.216144	0.000343

Cont

pot strain	stress	Mansur strain
0.001673	2.307629	0.000291
0.001721	2.399349	0.000285
0.001725	2.492720	0.000234
0.001780	2.583733	0.000234
0.001831	2.674746	0.000230
0.001852	2.766938	0.000196
0.001899	2.857715	0.000189
0.001917	2.948964	0.000152
0.001985	3.071808	0.000147
0.001900	3.163527	0.000007
0.001948	3.255013	0.000000
0.002075	3.433504	0.000020
0.002096	3.524045	-0.000013
0.002134	3.615294	-0.000029
0.002198	3.706069	-0.000020
0.002234	3.798732	-0.000040
0.002311	3.889981	-0.000017
0.002364	3.981467	-0.000019
0.002440	4.072246	0.000003
0.002508	4.162550	0.000017
0.002575	4.253799	0.000030

Appendix D - Toutanji Computations

The data provided in Table D.1 has information about the FRP as provided by the manufacturer converted into metric units as well as the values provided by Equation 11, and Equation 24 through Equation 27 which were used to calculate the first branch along with Equation 20 through Equation 23. The radial strain was systematically entered up to a strain of 0.013 inch/inch because this was the maximum that the strain gauges would be valid. Equation 10 calculates the lateral stress which is used in Equation 15 to calculate the stress for every point along the second branch which corresponds to Equation 19 for the strain along the second branch. These values were then combined and plotted.

Table D.1: Construction method for model

E_{frp}=	227527	Mpa
t=	0.1651	mm/ply
r=	76.2	mm
ε_r=	0.002	
E_l=	985.9503	Mpa
f'_{co}=	37.2179	Mpa
ε_{co}=	0.002	

$\varepsilon_{au(cu)}$	0.003452	
$f_{au(cu)}$	47.95309	
E_{ia}=	34055.25	Mpa
E_{ua}=	5722.252	Mpa

radial		*second branch*		*first branch*		*combined (ksi)*	
ε_r	f_l	$f_{c(MPa)}$	ε_c	ε_o	$f_{o\ (Mpa)}$	ε	$f_{o\ (ksi)}$
0.00000	0.00000	37.21790	0.00200	0.00000	0.00000	0.00000	0.00000
0.00001	0.00986	37.33660	0.00202	0.00001	0.33912	0.00001	0.04918
0.00002	0.01972	37.43186	0.00203	0.00002	0.67539	0.00002	0.09796
0.00003	0.02958	37.51990	0.00204	0.00003	1.00885	0.00003	0.14632
0.00004	0.03944	37.60356	0.00205	0.00004	1.33953	0.00004	0.19428
0.00005	0.04930	37.68411	0.00206	0.00005	1.66747	0.00005	0.24185
0.00006	0.05916	37.76226	0.00207	0.00006	1.99271	0.00006	0.28902
0.00007	0.06902	37.83847	0.00208	0.00007	2.31527	0.00007	0.33580
0.00008	0.07888	37.91306	0.00209	0.00008	2.63519	0.00008	0.38220
0.00009	0.08874	37.98626	0.00210	0.00009	2.95250	0.00009	0.42822
0.00010	0.09860	38.05824	0.00211	0.00010	3.26724	0.00010	0.47387
0.00011	0.10845	38.12916	0.00212	0.00011	3.57943	0.00011	0.51915
0.00012	0.11831	38.19911	0.00213	0.00012	3.88911	0.00012	0.56407
0.00013	0.12817	38.26819	0.00214	0.00013	4.19631	0.00013	0.60862
0.00014	0.13803	38.33648	0.00215	0.00014	4.50105	0.00014	0.65282
0.00015	0.14789	38.40404	0.00216	0.00015	4.80337	0.00015	0.69667
0.00016	0.15775	38.47092	0.00217	0.00016	5.10329	0.00016	0.74017
0.00017	0.16761	38.53719	0.00218	0.00017	5.40084	0.00017	0.78333
0.00018	0.17747	38.60287	0.00219	0.00018	5.69606	0.00018	0.82614
0.00019	0.18733	38.66800	0.00220	0.00019	5.98897	0.00019	0.86863

Appendix E - Berthet et al Computations

Table E.1 shows the values and computations used to construct the stress-strain diagram and compare the model's predictions with the test data.

Table E.1: Berthet et al computations

E_l=	985.9503	MPa
ε_{ao}=	0.002	
f'_{co} =	37.2179	MPa
f_{lu}=	16.46537	
f'_{cc}=	94.02343	MPa
ε_{au}=	0.020377	
θ_r=	2528.644	
$\varepsilon_r(\varepsilon_{rp})$=	0.002	
γ=	3.051849	
E_a*=	26736.66	

ε_{fu}=	0.0167	
t=	0.1651	mm/ply
r=	76.2	mm
k=	3.45	
E_{frp}=	227527	MPa
v_c=	0.2	
f'_{cp}=	56.852356	
E_c=	26659.83	MPa
ε_{ap}=	0.0025243	
E_r*=	137242.95	

combined branches			
strain	f'c (Mpa)	f'c (ksi)	
0.0000	0.0000	0.0000	
0.0001	2.743804	0.397955	
0.0002	5.619331	0.815015	
0.0003	8.611078	1.248931	
0.0004	11.70001	1.696942	
0.0005	14.86373	2.155801	
0.0006	18.07686	2.621827	
0.0007	21.31157	3.090981	
0.0008	24.53824	3.55897	
0.0009	27.72636	4.021367	
0.001	30.8454	4.473746	
0.0011	33.86579	4.911816	
0.0012	36.75985	5.331564	
0.0013	39.50261	5.729368	
0.0014	42.07252	6.102102	
0.0015	44.45198	6.447213	
0.0016	46.62762	6.762762	
0.0017	48.59041	7.047441	
0.0018	50.3356	7.30056	
0.0019	51.86244	7.522009	
0.002	53.17378	7.712203	
0.0021	54.2756	7.872009	
0.0022	55.17648	8.00267	
0.0023	55.88703	8.105726	
0.0024	56.41936	8.182934	
0.0025	56.78658	8.236196	
0.002524	56.85236	8.245735	transition pt

ultimate and transition points (in ksi)		
f'_{cp}=	8.2457349	
f'_{cc}=	13.636942	
ε_{ap}=	0.0025243	
ε_{au}=	0.0203768	

Appendix F - Teng and Lam Computations

Table F.1 shows the values used to construct the predicted stress-strain diagram which was then compared with the experimental data.

Table F.1: Teng and Lam Computations

$f'_{co}=f_o=$	5.398	ksi
$E_c=$	4187.852	ksi
$E_{frp}=$	33000	ksi
$\varepsilon_{h,\,rup}=$	0.009786	in/in
d=	6	in
t=	0.0065	in
$E_2=$	319.5638	ksi

$f_{la}=$	0.699713	ksi
$\varepsilon_{frp}=$	0.0167	in/in
$\varepsilon_{co}=$	0.002	in/in
$\varepsilon_{cu}=$	0.007226	in/in
$f'_{cc}=$	7.707054	ksi
$\varepsilon_t=$	0.002791	in/in

strain	stress
0.00000	0.00000
0.00001	0.04181
0.00002	0.08348
0.00003	0.12501
0.00004	0.16641
0.00005	0.20766
0.00006	0.24878
0.00007	0.28975
0.00008	0.33059
0.00009	0.37129
0.00010	0.41185
0.00011	0.45228
0.00012	0.49256
0.00013	0.53271
0.00014	0.57272
0.00015	0.61258